GFP and RFP fluorescence in tumors was imaged as described above. For some experiments, chemotherapy-resistant cancer cells were isolated by collagenase, and the isolated cells were cultured.

STATISTICAL ANALYSIS

All data represent the mean of at least three independent experiments ± SD. For the determination of statistical significance, the unpaired Student's *t*-tests, was used. *P*-values of less than 0.05 were considered statistically significant.

RESULTS AND DISCUSSION

COMPARATIVE BEHAVIOR OF CO-CULTURED COLOR-CODED CD133$^+$ AND CD133$^-$ HUH-7 HCC CELLS IN VITRO

Co-cultures of CD133$^+$ (CSC) and CD133$^-$ (NSCC) Huh-7 cells are shown in Figure 1. Approximately 49% of Huh-7 cells expressed CD133 (Fig. 1B). To compare the properties of Huh-7 CSCs and NSCCs, the same number of isolated GFP-CD133$^+$ and RFP-CD133$^-$ cells were co-cultured in dishes, and then GFP and RFP fluorescence was imaged. On days 0 and 1 after plating, both CD133$^+$ and CD133$^-$ Huh-7 cells showed similar morphology (Fig. 1C). From day 3, however, GFP CD133$^+$ cells became elongated and stretched (data not shown). In contrast, RFP CD133$^-$ cells showed minimal morphological change. Moreover, GFP CD133$^+$ cells showed higher proliferative activity than RFP CD133$^-$ cells 7 days after plating (Fig. 1D).

COMPARATIVE BEHAVIOR OF COLOR-CODED CD133$^+$ AND CD133$^-$ HUH-7 HCC CELLS IN THE SAME LIVER METASTASIS

To simultaneously image the properties of Huh-7 CD133$^+$ and CD133$^-$ cells in a tumor, an equal mixture of the two cell types was injected into the spleen of nude mice in order to obtain experimental liver metastasis. On day 1 after cell injection, GFP$^-$ and RFP$^-$

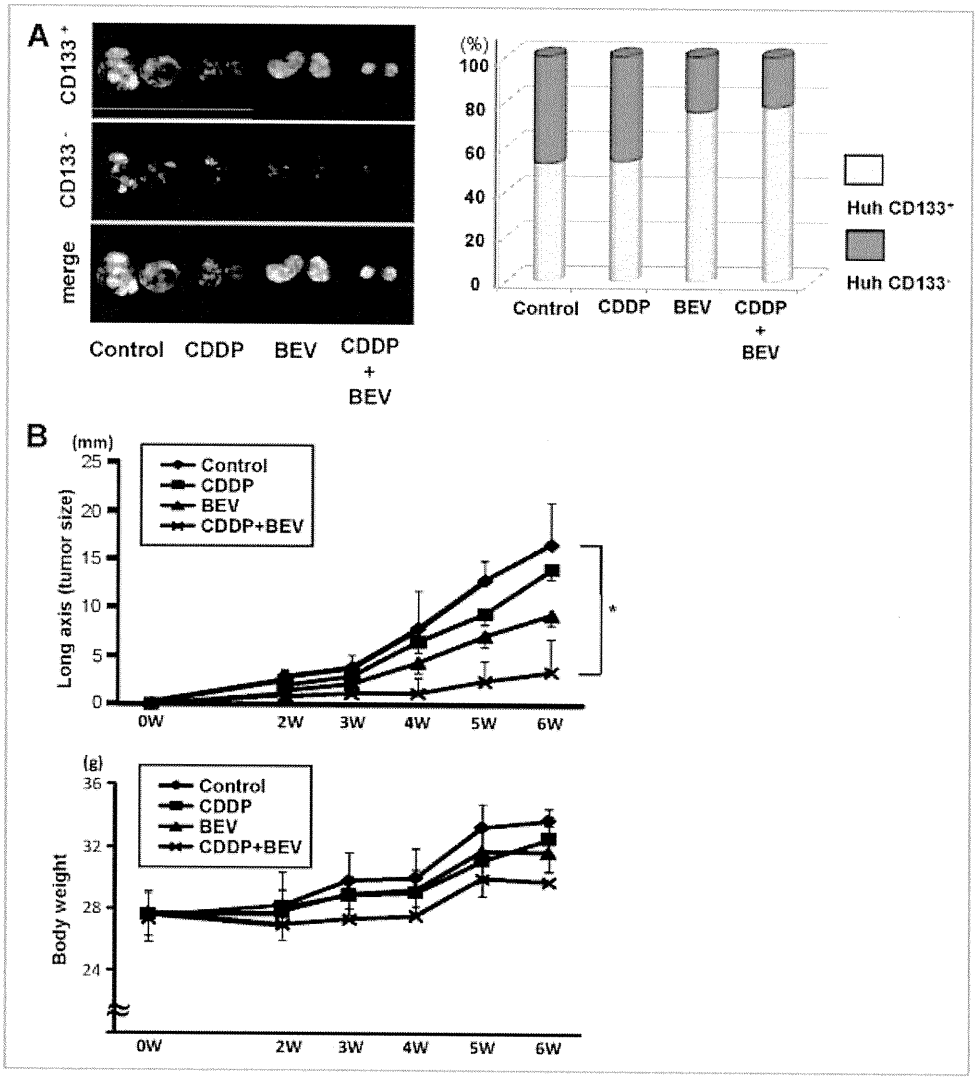

Fig. 3. The same number of isolated GFP-CSCs and RFP-NSCCs (1×10^6) were implanted subcutaneously in nude mice. The mice were treated with CDDP, BEV, or CDDP + BEV for 5 weeks from day 7 after implantation. A: The fluorescent areas of RFP and GFP were compared in the excised tumor. CD133$^+$ GFP-CSCs were more treatment resistant. B: Tumor size (longer axis) and body weight were measured. Data are means ± SD from at least 10 mice. $^*P < 0.01$ using the Student's *t*-test.

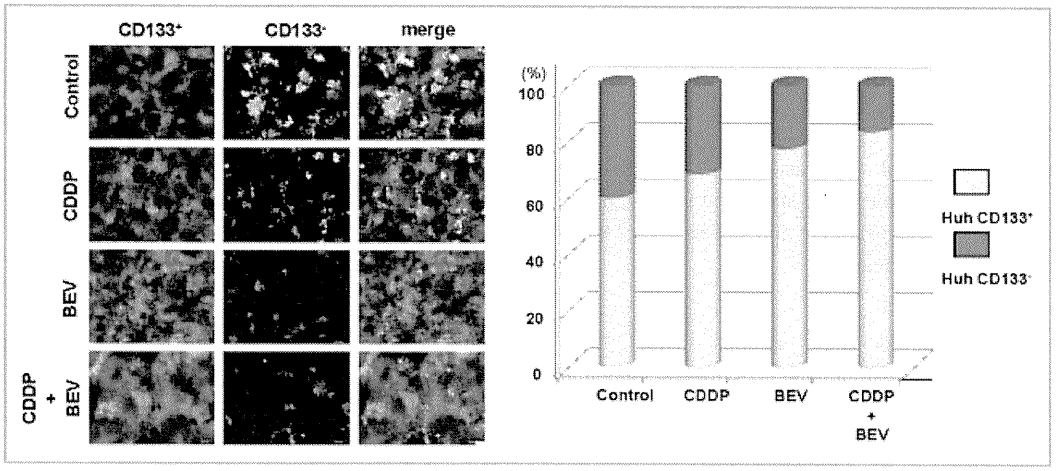

Fig. 4. The same number of isolated GFP-CSCs and RFP-NSCCs (1×10^6) were implanted subcutaneously in nude mice. The mice were treated with CDDP, BEV, or CDDP + BEV for 6 weeks from day 7 after implantation. The tumors were excised and treated with collagenase. The isolated cells (1×10^4) were cultured on plastic 64 well dishes. The total intensities of GFP and RFP fluorescence were compared in the wells 4 days after plating.

expressing cells were observed in the liver indicating the cancer cells began metastasizing to the liver. By day 28 after cell injection, very large multiple tumors were observed in the liver. GFP-expressing $CD133^+$ cells showed diffuse proliferation in the liver (Fig. 2). In contrast, RFP-expressing $CD133^-$ cells formed nodules on the liver (Fig. 2). The majority of the cells in the liver metastases were GFP $CD133^+$ cells, suggesting their greater ability to colonize the liver (Fig. 2). These results indicate that the $CD133^+$ showed enhanced migration and proliferation suggesting they are more malignant than the $CD133^-$ cells.

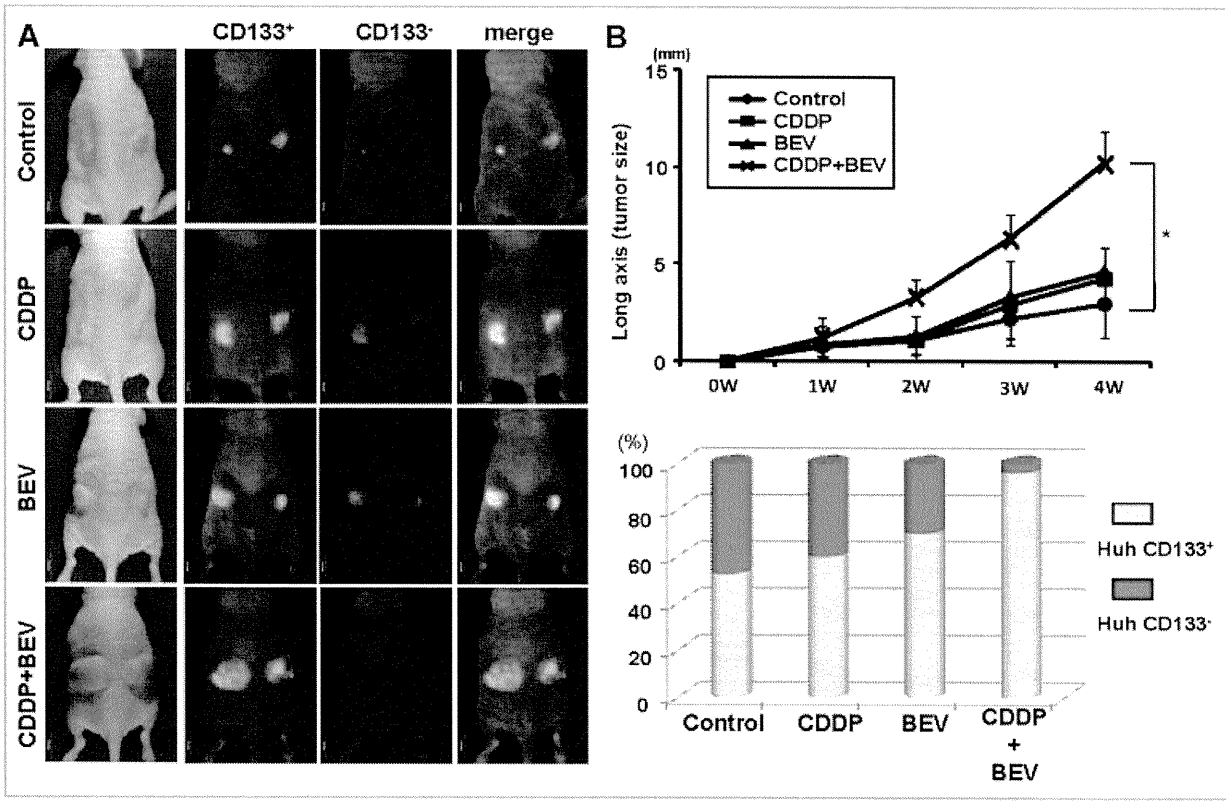

Fig. 5. The same number of the isolated GFP-CSCs and RFP-NSCCs (1×10^6) were implanted subcutaneously in nude mice. The mice were treated with CDDP, BEV, or CDDP + BEV for 6 weeks from day 7 after implantation. The tumors were excised and treated with collagenase. The isolated cells were cultured in plastic dishes. Four days after plating, the cultured cells (1×10^4) were subcutaneously implanted again into nude mice. A: Whole-body fluorescence images of animals were taken 4 weeks after implantation. The fluorescent areas of RFP and GFP were compared. B: Tumor size (longer axis) was measured at the indicated time points. Data are means ± SD from at least 10 mice. $^*P < 0.01$ using the Student's *t*-test.

COMPARATIVE CHEMOSENSITIVITY OF COLOR-CODED HUH-7 CD133$^+$ AND CD133$^-$ CELLS IN THE SAME TUMOR

To examine differential chemo-sensitivity of CSCs and NSCCs, the same number of isolated GFP CD133$^+$ and RFP-CD133$^-$ cells were implanted subcutaneously in nude mice. The mice were treated with CDDP, BEV, or CDDP + BEV beginning from day 7 after implantation. Chemotherapy reduced tumor growth, especially combination therapy with CDDP + BEV (Fig. 3A,B). The majority of the remaining cells in the tumors of CDDP + BEV treated mice were GFP-expressing CD133$^+$ suggesting that the CSCs were chemo-resistant.

Cells were isolated from the chemotherapy-treated subcutaneous tumors and cultured on plastic dishes. The ratio of GFP-expressing to RFP-expressing cells isolated from the non-treated group was $60.3 \pm 2.5\%$ to $39.6 \pm 2.5\%$ at 4 days after plating. In contrast, the ratio of GFP-expressing to RFP-expressing cells in CDDP + BEV treated group was $84 \pm 4\%$ to $16 \pm 4\%$ at 4 days after plating (Fig. 4) indicating that CD133$^+$ cells were highly resistant to the CDDP + BEV combination. GFP-CD133$^+$ also showed higher proliferative activity than RFP CD133$^-$ cells after isolation from CDDP + BEV-treated tumors. In contrast, the RFP-CD133$^-$ cells started to die and detach from the dish (data not shown) after plating, probably due to effects of the in vivo CDDP + BEV treatment.

To further investigate the properties of the chemotherapy-resistant cells, the same number of control or chemotherapy resistant cells isolated and cultured from subcutaneous tumors were implanted again into nude mice. The CDDP + BEV-resistant cells formed the largest tumors (Fig. 5A). In these tumors, GFP-CD133$^+$ cells were found to be more predominant than RFP-CD133$^-$ cells. The ratio of GFP-CD133$^+$ to RFP-CD133$^-$ in the tumors formed from the cells isolated and cultured from the control group was $59.6 \pm 5.1\%$ to $40.3 \pm 5.1\%$. In contrast, the ratio of GFP-CD133$^+$ to RFP-CDD133$^-$ cells isolated and cultured from the CDDP + BEV-treated groups was $96.33 \pm 1.5\%$ to $3.66 \pm 1.5\%$ (Fig. 5B). These results demonstrate that the viable CDDP + BEV-resistant cells were almost all CD133$^+$.

In the present study, we could differentiate between CSCs and NSCCs in the same tumor using different colored fluorescent proteins to label CSCs and NSCCs and then perform color-coded imaging. We demonstrated striking differences in cell proliferation, metastasis, and drug sensitivity between CD133$^+$ and CD133$^-$ cells. Our results demonstrate that Huh-7 CD133$^+$ have at least some properties of cancer stem cells.

Labeling CSC with GFP and NSCC with RFP allows imaging of CSC and NSCC interaction as well as interaction of each cell type with the host.

The present report now enables cancer stem-like cells to be characterized and distinguished from non-stem cells in the same tumor in real time with regard to the most important features of malignancy. Our results confirm that tumors can contain two very different populations with regard to malignancy and drug sensitivity. However, the malignant cell set (stem-cell like) is not a rare population in Huh-7 tumors. Imageable CSC can be a visual target to prevent metastasis, which would be of great importance for adjuvant chemotherapy. Future studies will focus on selective in vivo labeling of CSC visual targets of chemotherapy [Kishimoto et al., 2009a,b].

ACKNOWLEDGMENTS

This work was supported in part by funding from National Cancer Institute grant CA132971.

REFERENCES

Abraham BK, Fritz P, McClellan M, Hauptvogel P, Athelogou M, Brauch H. 2005. Prevalence of CD44+/CD24−/low cells in breast cancer may not be associated with clinical outcome but may favor distant metastasis. Clin Cancer Res 11:1154–1159.

Al-Hajj M, Wicha MS, Benito-Hernandez A, Morrison SJ, Clarke MF. 2003. Prospective identification of tumorigenic breast cancer cells. Proc Natl Acad Sci USA 100:3983–3988.

Bao S, Wu Q, McLendon RE, Hao Y, Shi Q, Hjelmeland AB, Dewhirst MW, Bigner DD, Rich JN. 2006. Glioma stem cells promote radioresistance by preferential activation of the DNA damage response. Nature 444:756–760.

Bjerkvig R, Tysnes BB, Aboody KS, Najbauer J, Terzis AJ. 2005. Opinion: The origin of the cancer stem cell: Current controversies and new insights. Nat Rev Cancer 5:899–904.

Bonnet D, Dick JE. 1997. Human acute myeloid leukemia is organized as a hierarchy that originates from a primitive hematopoietic cell. Nat Med 3:730–737.

Bussolati B, Bruno S, Grange C, Buttiglieri S, Deregibus MC, Cantino D, Camussi G. 2005. Isolation of renal progenitor cells from adult human kidney. Am J Pathol 166:545–555.

Chishima T, Miyagi Y, Wang X, Yamaoka H, Shimada H, Moossa AR, Hoffman RM. 1997. Cancer invasion and micrometastasis visualized in live tissue by green fluorescent protein expression. Cancer Res 57:2042–2047.

Dean M, Fojo T, Bates S. 2005. Tumour stem cells and drug resistance. Nat Rev Cancer 5:275–284.

Donnenberg VS, Landreneau RJ, Donnenberg AD. 2007. Tumorigenic stem and progenitor cells: Implications for the therapeutic index of anti-cancer agents. J Control Release 122:385–391.

Hoffman RM. 2005. The multiple uses of fluorescent proteins to visualize cancer in vivo. Nat Rev Cancer 5:796–806.

Hoffman RM, Yang M. 2006a. Subcellular imaging in the live mouse. Nat Protoc 1:775–782.

Hoffman RM, Yang M. 2006b. Color-coded fluorescence imaging of tumor-host interactions. Nat Protoc 1:928–935.

Hoffman RM, Yang M. 2006c. Whole-body imaging with fluorescent proteins. Nat Protoc 1:1429–1438.

Jaszai J, Fargeas CA, Florek M, Huttner WB, Corbeil D. 2007. Focus on molecules: Prominin-1 (CD133). Exp Eye Res 85:585–586.

Jordan CT, Guzman ML, Noble M. 2006. Cancer stem cells. N Engl J Med 355:1253–1261.

Kishimoto H, Zhao M, Hayashi K, Urata Y, Tanaka N, Fujiwara T, Penman S, Hoffman RM. 2009a. In vivo internal tumor illumination by telomerase-dependent adenoviral GFP for precise surgical navigation. Proc Natl Acad Sci USA 106:14514–14517.

Kishimoto H, Urata Y, Tanaka N, Fujiwara T, Hoffman RM. 2009b. Selective metastatic tumor labeling with green fluorescent protein and killing by systemic administration of telomerase-dependent adenoviruses. Mol Cancer Ther 8:3001–3008.

Ma S, Chan KW, Hu L, Lee TK, Wo JY, Ng IO, Zheng BJ, Guan XY. 2007. Identification and characterization of tumorigenic liver cancer stem/progenitor cells. Gastroenterology 132:2542–2556.

Miki J, Furusato B, Li H, Gu Y, Takahashi H, Egawa S, Sesterhenn IA, McLeod DG, Srivastava S, Rhim JS. 2007. Identification of putative stem cell markers, CD133 and CXCR4, in hTERT-immortalized primary nonmalignant and malignant tumor-derived human prostate epithelial cell lines and in prostate cancer specimens. Cancer Res 67:3153–3161.

Mizrak D, Brittan M, Alison MR. 2008. CD133: Molecule of the moment. J Pathol 214:3–9.

Monzani E, Facchetti F, Galmozzi E, Corsini E, Benetti A, Cavazzin C, Gritti A, Piccinini A, Porro D, Santinami M, Invernici G, Parati E, Alessandri G, La Porta CA. 2007. Melanoma contains CD133 and ABCG2 positive cells with enhanced tumourigenic potential. Eur J Cancer 43:935–946.

O'Brien CA, Pollett A, Gallinger S, Dick JE. 2007. A human colon cancer cell capable of initiating tumour growth in immunodeficient mice. Nature 445:106–110.

Reya T, Morrison SJ, Clarke MF, Weissman IL. 2001. Stem cells, cancer, and cancer stem cells. Nature 414:105–111.

Ricci-Vitiani L, Lombardi DG, Pilozzi E, Biffoni M, Todaro M, Peschle C, De Maria R. 2007. Identification and expansion of human colon-cancer-initiating cells. Nature 445:111–115.

Suetsugu A, Nagaki M, Aoki H, Motohashi T, Kunisada T, Moriwaki H. 2006. Characterization of CD133+ hepatocellular carcinoma cells as cancer stem/progenitor cells. Biochem Biophys Res Commun 351:820–824.

Tome Y, Tsuchiya H, Hayashi K, Yamauchi K, Sugimoto N, Kanaya F, Tomita K, Hoffman RM. 2009. In vivo gene transfer between interacting human osteosarcoma cell lines is associated with acquisition of enhanced metastatic potential. J Cell Biochem 108:362–367.

Toren A, Bielorai B, Jacob-Hirsch J, Fisher T, Kreiser D, Moran O, Zeligson S, Givol D, Yitzhaky A, Itskovitz-Eldor J, Kventsel I, Rosenthal E, Amariglio N, Rechavi G. 2005. CD133-positive hematopoietic stem cell "stemness" genes contain many genes mutated or abnormally expressed in leukemia. Stem Cells 23:1142–1153.

Yamauchi K, Yang M, Jiang P, Xu M, Yamamoto N, Tsuchiya H, Tomita K, Moossa AR, Bouvet M, Hoffman RM. 2006. Development of real-time subcellular dynamic multicolor imaging of cancer-cell trafficking in live mice with a variable-magnification whole-mouse imaging system. Cancer Res 66:4208–4214.

Yang M, Baranov E, Jiang P, Sun FX, Li XM, Li L, Hasegawa S, Bouvet M, Al-Tuwaijri M, Chishima T, Shimada H, Moossa AR, Penman S, Hoffman RM. 2000. Whole-body optical imaging of green fluorescent protein-expressing tumors and metastases. Proc Natl Acad Sci USA 97:1206–1211.

Yin AH, Miraglia S, Zanjani ED, Almeida-Porada G, Ogawa M, Leary AG, Olweus J, Kearney J, Buck DW. 1997. AC133, a novel marker for human hematopoietic stem and progenitor cells. Blood 90:5002–5012.

Yin S, Li J, Hu C, Chen X, Yao M, Yan M, Jiang G, Ge C, Xie H, Wan D, Yang S, Zheng S, Gu J. 2007. CD133 positive hepatocellular carcinoma cells possess high capacity for tumorigenicity. Int J Cancer 120:1444–1450.

DOI:10.1158/1078-0432.CCR-08-2093

Supplementation with Branched-chain Amino Acids Inhibits Azoxymethane-induced Colonic Preneoplastic Lesions in Male C57BL/KsJ-*db/db* Mice

Masahito Shimizu,[1] Yohei Shirakami,[1] Junpei Iwasa,[1] Makoto Shiraki,[1] Yoichi Yasuda,[1] Kazuya Hata,[3] Yoshinobu Hirose,[2] Hisashi Tsurumi,[1] Takuji Tanaka,[4] and Hisataka Moriwaki[1]

Abstract **Purpose:** Obesity and related metabolic abnormalities, including insulin resistance and activation of the insulin-like growth factor (IGF)/IGF-I receptor (IGF-IR) axis, are risk factors for colon cancer. Supplementation with branched-chain amino acids (BCAA) reduces the risk of liver cancer in cirrhotic patients who are obese, and this has been associated with an improvement of insulin resistance. The present study examined the effects of BCAA on the development of azoxymethane (AOM)-initiated colonic premalignant lesions in C57BL/KsJ-*db/db* (*db/db*) mice that were obese and had hyperinsulinemia.

Experimental Design: Male *db/db* mice were given 4 weekly s.c. injections of AOM (15 mg/kg of body weight) and then they were fed a diet containing 3.0% BCAA or casein, a nitrogenc content–matched control diet, for 7 weeks.

Results: Feeding with BCAA caused a significant reduction in the number of total aberrant crypt foci and β-catenin accumulated crypts, both of which are premalignant lesions of the colon, compared with the control diet–fed groups. BCAA supplementation caused a marked decrease in the expression of IGF-IR, the phosphorylated form of IGF-IR, phosphorylated glycogen synthase kinase 3β, phosphorylated Akt, and cyclooxygenase-2 proteins on the colonic mucosa of AOM-treated mice. The serum levels of insulin, IGF-I, IGF-II, triglyceride, total cholesterol, and leptin were also decreased by supplementation with BCAA.

Conclusion: BCAA supplementation in diet improves insulin resistance and inhibits the activation of the IGF/IGF-IR axis, thereby preventing the development of colonic premalignancies in an obesity-related colon cancer model that was also associated with hyperlipidemia and hyperinsulinemia. BCAA, therefore, may be a useful chemoprevention modality for colon cancer in obese people.

Colorectal cancer (CRC) is a major health problem worldwide. Recent evidence indicates that the risk of CRC is elevated in patients with metabolic syndrome, also called insulin resistance syndrome, which is commonly associated with obesity and related metabolic abnormalities (1, 2). Obesity is the main determinant of insulin resistance and hyperinsulinemia, which is also a possible risk factor for CRC (3). CRC occurs more frequently in patients with diabetes mellitus, a condition associated with hyperinsulinemia (4, 5). Insulin has growth-promoting properties in CRC cells, and exogenous insulin injection stimulates the growth of CRC precursors in rodent models (6–8). In addition, elevated circulating levels of insulin causes alterations in the insulin-like growth factor (IGF)/IGF-I receptor (IGF-IR) axis, which is involved in the development and progression of CRC (9, 10). Therefore, increased insulin resistance and abnormalities in the IGF/IGF-IR axis might be a critical target to prevent the development of obesity-related malignancies, including CRC. For instance, (-)-epigallocatechin gallate, the major biologically active component of green tea, inhibited the development of colonic premalignant lesions in an obesity-related colon cancer that was associated with improvement in insulin resistance and inhibition of the IGF/IGF-IR axis (11).

Diet supplementation with branched-chain amino acids (BCAA; leucine, isoleucine, and valine) has been suggested to improve protein malnutrition in patients with liver cirrhosis (12). Recent studies have revealed that BCAA is useful for both preventing progressive hepatic failure and improving event-free survival in patients with chronic liver diseases, such as liver cirrhosis, and these beneficial effects are associated with the improvement of insulin resistance by BCAA (13–15). In addition, oral supplemental treatment with BCAA can reduce the risk of hepatocellular carcinoma in cirrhotic patients who

Authors' Affiliations: [1]Departments of Medicine and [2]Tumor Pathology, Gifu University Graduate School of Medicine; [3]BMR Laboratories, Sunplanet Co., Ltd, Gifu, Japan; and [4]Department of Oncologic Pathology, Kanazawa Medical University, Ishikawa, Japan

Received 8/10/08; revised 1/8/09; accepted 1/23/09; published OnlineFirst 4/14/09.
Grant support: Ministry of Education, Science, Sports and Culture of Japan Grants-in-Aid Nos. 18790457 (M. Shimizu) and 17015016 (H. Moriwaki).
The costs of publication of this article were defrayed in part by the payment of page charges. This article must therefore be hereby marked *advertisement* in accordance with 18 U.S.C. Section 1734 solely to indicate this fact.

Requests for reprints: Masahito Shimizu, Department of Medicine, Gifu University Graduate School of Medicine, 1-1 Yanagido, Gifu 501-1194, Japan. Phone: 81-58-230-6313; Fax: 81-58-230-6310; E-mail: shimim-gif@umin.ac.jp.

©2009 American Association for Cancer Research.

doi:10.1158/1078-0432.CCR-08-2093

DOI:10.1158/1078-0432.CCR-08-2093

Translational Relevance

Obesity and related metabolic abnormalities, including insulin resistance and the activation of the insulin-like growth factor (IGF)/IGF-I receptor axis, are associated with colorectal cancer (CRC) development. Therefore, the prevention of CRC by targeting the dysregulation of energy homeostasis might be a promising strategy for obese people who are at increased risks of CRC. We believe that this study is novel and clinically relevant because this article is the first report indicating that supplementation with branched-chain amino acids (BCAA) effectively suppressed the development of azoxymethane-induced putative precursor lesions of colonic adenocarcinoma in C57BL/KsJ-*db/db* mice that are obese and developed diabetes mellitus. Our studies indicate that this suppressing effect of BCAA was associated with improvement of hyperlipidemia and hyperleptinemia. BCAA supplementation could also improve insulin resistance and exert a depressant effect on the IGF/IGF-IR axis. The current findings suggest the possibility of using BCAA as a chemopreventive agent for obesity-related malignancies.

are obese (with a body mass index ≥25; ref. 16). Obesity, hyperinsulinemia, and diabetes mellitus are possible risk factors for hepatocellular carcinoma, which commonly develops in cirrhotic livers (16–18). Based on these findings, BCAA supplementation in diet may also reduce the risk of other obesity-related human malignancies, including CRC, by improving insulin resistance. However, no detailed studies on whether BCAA can prevent the development of obesity-related CRC have yet been conducted.

In previous studies, we have established a useful preclinical animal model to determine the possible underlying mechanisms of how specific agents prevent the development of obesity-related CRC with the use of C57BL/KsJ-*db/db* (*db/db*) mice with obesity, hyperinsulinemia, and hyperleptinemia (19–21). The mice are susceptible to the colonic carcinogen azoxymethane (AOM) because the development of AOM-induced aberrant crypt foci (ACF) and β-catenin–accumulated crypts (BCAC), both of which are putative precursor lesions for colonic adenocarcinoma (22, 23), is enhanced in *db/db* mice compared with *db*/+ or +/+ mice (19, 20). In the present study, we investigated in detail the effects of BCAA on the development of colonic premalignant lesions, ACF and BCAC, in *db/db* mice initiated with AOM, focusing on the improvement of hyperinsulinemia, hyperlipidemia, and hyperleptinemia. In addition, we also determined whether BCAA supplementation in the diet inhibits the activation of the IGF/IGF-IR axis in this animal model.

Materials and Methods

Animals, chemicals, and diets. Four-week-old male homozygous *db/db* mice were obtained from Japan SLC, Inc.. All mice were maintained at the Gifu University Life Science Research Center according to the Institutional Animal Care Guidelines. AOM was purchased from Sigma Chemical Co.. BCAA and casein were obtained from Ajinomoto Co., Ltd.. The BCAA composition (2:1:1.2, leucine/isoleucine/valine) was set at the clinical dosage that is used for the treatment of hypoalbuminemia in patients with decompensated liver cirrhosis in Japan.

Experimental procedure. The animal experiment was approved by the Institutional Committee of Animal Experiments of Gifu University. A total of 54 male *db/db* mice were divided into 6 groups. At 5 wk of age, the mice in groups 1 to 3 were s.c. injected with AOM (15 mg/kg of body weight) weekly for 4 wk. As controls, the mice in groups 4 to 6 were given s.c. injections of saline. Groups 1 (12 mice) and 4 (6 mice) were fed a basal diet, corticotropin-releasing factor (CRF)-1 (Oriental Yeast Co., Ltd.), throughout the experiment. Groups 3 (12 mice) and 6 (6 mice) were given a basal diet containing 3.0% BCAA (weight for weight) for 7 wk, starting 1 wk after the last injection of AOM. The BCAA concentration (3.0%) was determined by the previous study, which indicated the same intake to improve insulin resistance in C57BL/6J mice (24). The mice in groups 2 (12 mice) and 5 (6 mice) were given a basal diet containing 3.0% casein (weight for weight). The casein-fed groups were served as nitrogen content–matched controls for the BCAA-treated groups to eliminate the possibility that the nitrogen content itself affects the promotion or the prevention of colonic premalignant lesions. At the termination of the study (16 wk of age), the mice were sacrificed by CO_2 asphyxiation to analyze the number of colonic ACF and BCAC.

Counting the number of ACF and BCAC. The ACF and BCAC were determined according to the standard procedures described previously (20, 21, 25). ACF are defined as single or multiple crypts that have altered luminal openings, exhibit thickened epithelia, and are larger than adjacent normal crypts (22). BCAC, which have high frequency mutations in the *β-catenin* gene, show histologic dysplasia with a disruption of the cellular morphology and an accumulation of this protein (Fig. 1A; ref. 23). BCAC do not have a typical ACF-like appearance because the lesion is not recognized on the mucosal surface like ACF and is only identified in the histologic sections of en face preparations. Both of these lesions are utilized as biomarkers to evaluate a number of agents for their potential chemopreventive properties (26). After the colons were fixed flat in 10% buffered formalin for 24 h, the mucosal surface of the colons were stained with methylene blue (0.5% in distilled water), and then the number of ACF were counted under a light microscope. Thereafter, the distal parts (5 cm from the anus) of the colon were cut to count the number of BCAC. To identify BCAC intramucosal lesions, the distal part of the colon (mean area, 0.7 cm^2 per colon) was embedded in paraffin, and then a total of 20 serial sections (4-μm thick each) per colon were made by an en face preparation (20, 21, 25). For each case, 2 serial sections were used to analyze BCAC.

Histopathology and immunohistochemical analyses for β-catenin and PCNA. Three serial sections were made from paraffin-embedded tissue blocks. Two sections were subjected to H&E staining for histopathology and β-catenin immunohistochemistry to count the number of BCAC. The other section was used for the proliferating cell nuclear antigen (PCNA), a G_1-to-S phase marker, immunohistochemistry to estimate the cell proliferative activity in the colonic mucosa. Immunohistochemical analyses for β-catenin and PCNA were done with the labeled streptavidin-biotin method (LSAB kit; DAKO) as previously described (20, 21). Anti–β-catenin antibody (1:1,000 final dilution) was obtained from Transduction Laboratories (catalogue no. 610154). Anti-PCNA antibody (1:100 final dilution) was from Santa Cruz Biotechnology, Inc. (sc-7907). Negative control sections were immunostained without the primary antibody. PCNA-positive cells in the colonic mucosa, which seemed normal by H&E staining, were counted and expressed as a percentage of the total number of normal crypt cells. The PCNA labeling index (%) was determined by counting at least 200 crypt cells in each mouse (a total of 1,000 crypt cells per group). Two experienced pathologists (Y. Hirose and T. Tanaka) immunohistologically determined the BCAC and PCNA-positive cells.

Protein extraction and western blot analysis. Total proteins were extracted from the scraped mucosa from the remaining colon of the AOM-treated mice (groups 1 to 3), and equivalent amounts of proteins

DOI:10.1158/1078-0432.CCR-08-2093

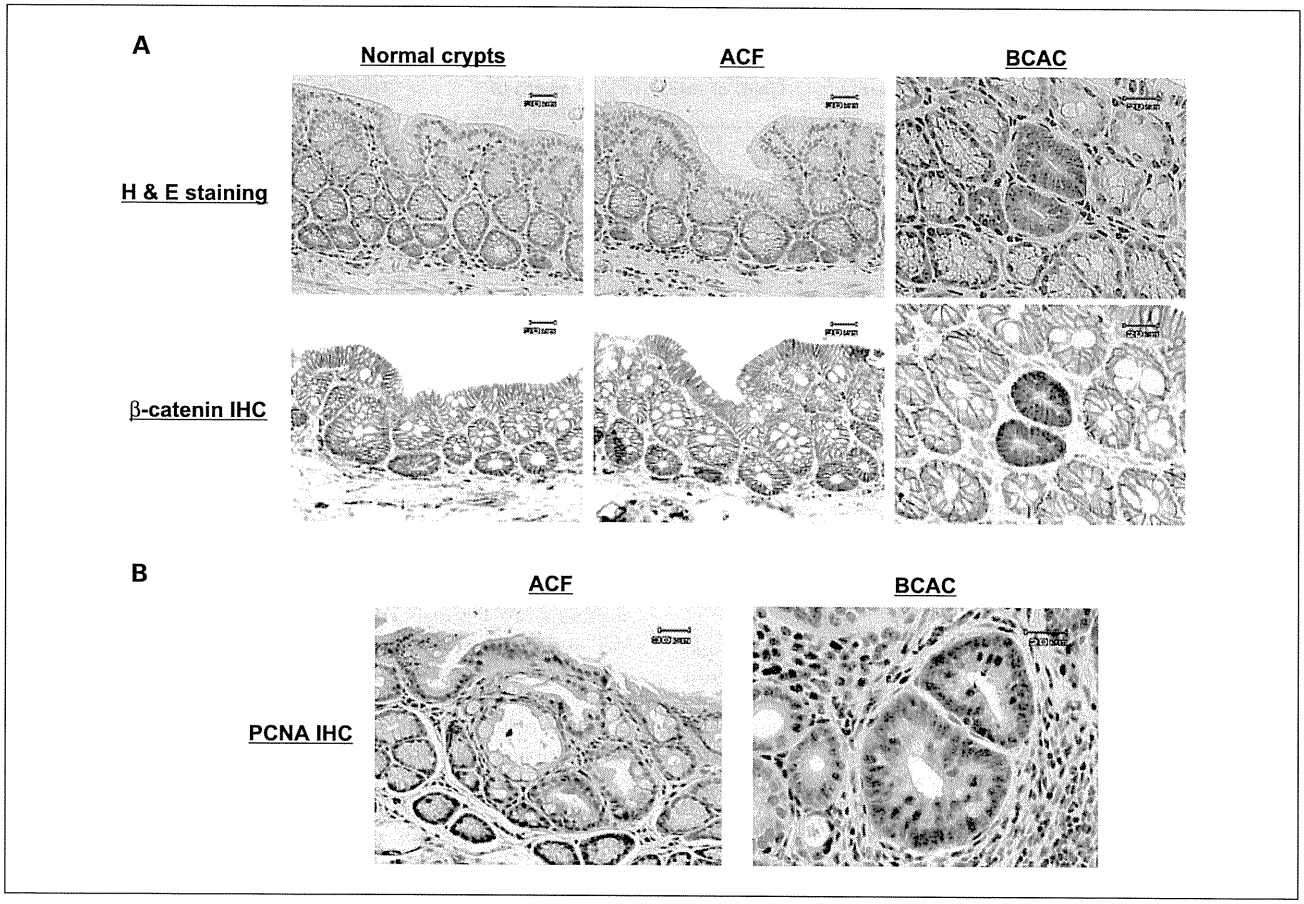

Fig. 1. Histopathology and immunohistochemical expression of β-catenin and PCNA proteins in ACF and BCAC. *A,* representative photographs of ACF and BCAC induced by AOM in *db/db* mice. Top, H&E staining; bottom, β-catenin immunohistochemistry. Left, normal crypts; middle, ACF; right, BCAC. The localization of the accumulated β-catenin protein is apparent in the cytoplasm and nucleus of atypical cryptal cells in BCAC. *B,* immunohistochemical pattern of PCNA protein in ACF and BCAC. The nuclear expression of the PCNA protein significantly increased in BCAC compared with ACF and surrounding normal crypts. Bar, 20 or 30 μm, respectively.

(40 μg per lane) were examined by a western blot analysis with the use of the primary antibodies for IGF-IR, phosphorylated IGF-IR (p-IGF-IR), phosphorylated glycogen synthase kinase 3β (p-GSK-3β), Akt, phosphorylated Akt (p-Akt), cyclooxygenase-2 (COX-2), and glyceraldehyde-3-phosphate dehydrogenase as described previously (11, 27, 28). An antibody to glyceraldehyde-3-phosphate dehydrogenase served as a loading control. The intensities of the blots were quantified with the NIH Image software version 1.62. The intensities of the blots found at the CRF-fed mice in each antibody was set at 1, and the changes in expression were shown as the fold difference.

Table 1. Body, liver, kidney, and white adipose tissue weights of the experimental mice

Group no.	Treatment	Diet	No. of mice	Final body weight (g)	Body length (cm)	BMI	Absolute organ weight		
							Liver	Kidney	White adipose tissue
1	AOM 15 mg/kg	CRF-1	12	49.7 ± 8.3*,†	9.25 ± 0.77	0.58 ± 0.05	2.64 ± 0.76	0.38 ± 0.04†	2.67 ± 0.64
2	AOM 15 mg/kg	Casein	12	51.7 ± 4.8	9.43 ± 0.37	0.58 ± 0.02	2.75 ± 0.48‡	0.41 ± 0.04	2.74 ± 0.37
3	AOM 15 mg/kg	BCAA	12	50.3 ± 5.0§	9.47 ± 0.25	0.56 ± 0.04	2.58 ± 0.64§	0.40 ± 0.05	2.51 ± 0.42
4	Saline	CRF-1	6	58.1 ± 2.5	9.63 ± 0.22	0.63 ± 0.02	3.35 ± 0.72	0.45 ± 0.06	3.02 ± 0.32
5	Saline	Casein	6	58.0 ± 2.1	9.70 ± 0.18	0.62 ± 0.01	3.87 ± 1.04	0.44 ± 0.04	2.70 ± 0.38
6	Saline	BCAA	6	58.5 ± 2.5	9.63 ± 0.17	0.63 ± 0.01	3.83 ± 0.86	0.44 ± 0.01	2.60 ± 0.35

*Mean ± SD.
†Significantly different from group 4 ($P < 0.05$).
‡Significantly different from group 5 ($P < 0.05$).
§Significantly different from group 6 ($P < 0.05$).

DOI:10.1158/1078-0432.CCR-08-2093

Table 2. Effects of BCAA on AOM-induced ACF and BCAC formation in the experimental mice

Group no.	Treatment	Diet	No. of mice	Length of colon (cm)	Total no. of ACFs per colon	Total no. of BCACs/cm^2
1	AOM 15 mg/kg	CRF-1	12	12.4 ± 1.4*	85.9 ± 8.1	11.7 ± 8.4
2	AOM 15 mg/kg	Casein	12	12.5 ± 0.5	83.4 ± 11.2	8.3 ± 3.9
3	AOM 15 mg/kg	BCAA	12	12.0 ± 0.7	54.5 ± 8.6†,‡	4.2 ± 6.7§
4	Saline	CRF-1	6	12.5 ± 1.0	0	0
5	Saline	Casein	6	11.5 ± 0.7	0	0
6	Saline	BCAA	6	11.3 ± 0.5	0	0

*Mean ± SD.
†Significantly different from group 1 ($P < 0.001$).
‡Significantly different from group 2 ($P < 0.001$).
§Significantly different from group 1 ($P < 0.05$).

Clinical chemistry. At sacrifice, blood samples were collected from the AOM-treated mice (groups 1-3) to measure the serum concentrations of insulin, leptin, triglyceride, total cholesterol, IGF-I, IGF-II, and BCAA. The serum triglyceride, total cholesterol, and BCAA levels were assayed as described previously (20, 29). The serum insulin, leptin, IGF-I, and IGF-II were determined by an enzyme immunoassay according to the manufacturer's protocol (R&D Systems).

Statistical analysis. The results were presented as the mean ± SD and were analyzed with the use of the GraphPad InStat software program version 3.05 (GraphPad Software) for Macintosh. Differences between groups were analyzed by one-way ANOVA or, as required, by two-way ANOVA. When ANOVA showed a statistically significant effect ($P < 0.05$), comparisons of each experimental group with the control group were then made with the use of the Tukey-Kramer multiple comparisons test. The differences were considered significant when the two-tailed P was <0.05.

Results

General observations. As shown in Table 1, the average body weights of groups 1 (CRF-1) and 3 (BCAA) in the AOM-injected mice at the termination of this experiment were smaller than those of the saline-injected groups 4 (CRF-1; $P < 0.05$) and 6 (BCAA; $P < 0.05$). The mean liver weights in the AOM-treated groups 2 (casein) and 3 (BCAA) were significantly lower than those in the saline-treated groups 5 (casein; $P < 0.05$) and 6 (BCAA; $P < 0.05$). Among CRF-1–fed mice, the mean kidney weight in the AOM-treated group 1 was also significantly lower than that of the saline-treated group 4 ($P < 0.05$). No significant difference was observed in the body length, body mass index, and mean white adipose tissue weight among the experimental mice. A histopathologic examination also revealed no alteration, thus suggesting the absence of toxicity of BCAA in the liver and kidney of the mice in groups 3 and 6 (data not shown).

Effects of BCAA supplementation on AOM-induced ACF and BCAC formations in db/db *mice.* Table 2 summarizes the total number of ACF and BCAC (Fig. 1) in the mice of all groups. ACF and BCAC developed in the colons of all the mice that received AOM (groups 1 to 3) but not in the colons of the mice that did not receive AOM (groups 4 to 6). Dietary supplementation with BCAA significantly decreased the number of total ACF compared with those of the CRF-1–fed (37% reduction; $P < 0.001$) and casein-supplemented groups (35% reduction; $P < 0.001$). Compared with the CRF-1–fed group, the administration of BCAA also significantly reduced the number of total BCAC (64% reduction; $P < 0.05$).

Effects of BCAA supplementation on the serum levels of BCAA in AOM-treated db/db *mice.* Because the colonic premalignant lesions developed only in the AOM-injected mice (Table 2), the following experiments were done among the mice thatz received AOM (groups 1 to 3). BCAA supplementation caused a significant increase in the serum concentrations of total BCAA (valine, isoleucine, and leucine; 1736 ± 179 nmol/mL) compared with the CRF-1–fed (882 ± 160 nmol/mL; $P < 0.001$) and casein-supplemented groups (853 ± 51 nmol/mL; $P < 0.001$). These findings suggest that supplementation with 3.0% BCAA is sufficient to raise the serum concentration of BCAA.

Effects of BCAA supplementation on the serum levels of total cholesterol, triglyceride, and leptin in AOM-treated db/db *mice.* As shown in Table 3, the serum levels of total cholesterol in the BCAA-supplemented mice were significantly lower than

Table 3. Serum levels of total cholesterol, triglyceride, and leptin in AOM-treated *db/db* mice

Group no.	Treatment	Diet	No. of mice	Total cholesterol (mg/dL)	Triglyceride (mg/dL)	Leptin (ng/dL)
1	AOM 15 mg/kg	CRF-1	12	185 ± 34*	244 ± 49	117 ± 18
2	AOM 15 mg/kg	Casein	12	186 ± 40	229 ± 40	133 ± 32
3	AOM 15 mg/kg	BCAA	12	141 ± 48†,‡	187 ± 48†	99 ± 23§

*Mean ± SD.
†Significantly different from group 1 ($P < 0.05$).
‡Significantly different from group 2 ($P < 0.05$).
§Significantly different from group 2 ($P < 0.01$).

DOI:10.1158/1078-0432.CCR-08-2093

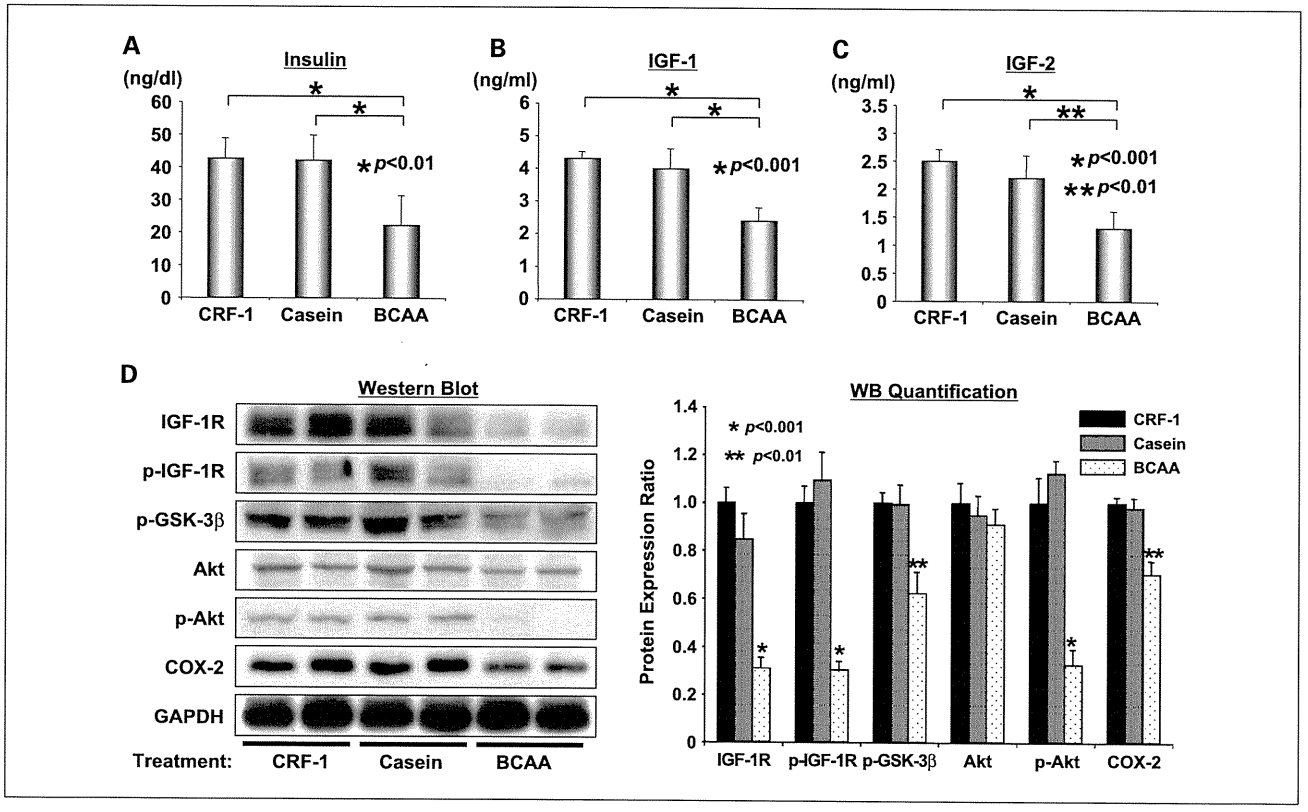

Fig. 2. The effect of BCAA supplementation on the serum levels of insulin, IGF-I, and IGF-II, and on the expression levels of the IGF-IR, p-IGF-IR, p-GSK-3β, Akt, p-Akt, and COX-2 proteins in AOM-treated *db/db* mice. *A* to *C*, the serum concentration of insulin (*A*), IGF-I (*B*), and IGF-II (*C*) were measured by an enzyme immunoassay. Bars, SD of triplicate assays. *D*, total proteins were extracted from the scraped colonic mucosa, and equivalent amounts of proteins were examined by a western blot analysis as described in Materials and Methods. Lanes, protein samples from two different mice in each group (*left*). The intensities of blots were quantitated by densitometry (*right*). Repeat western blots gave similar results. Values, mean ± SD. *, $P < 0.001$ and **, $P < 0.01$: significant differences obtained by comparison with CRF-1 – treated or casein-treated mice, respectively.

those in the CRF-1 – fed ($P < 0.05$) and casein-supplemented mice ($P < 0.05$). The mice supplemented with BCAA showed a significant decrease in the serum levels of triglyceride compared with the CRF-1 fed ($P < 0.05$). The serum leptin level of group 3 (BCAA) was also significantly lower than that of group 2 (casein; $P < 0.01$).

Effects of BCAA supplementation on the serum levels of insulin, IGF-I, and IGF-II in AOM-treated db/db *mice.* Supplementation with BCAA caused a significant decrease in the serum levels of insulin (Fig. 2A) compared with the CRF-1 – fed ($P < 0.01$) and casein-supplemented mice ($P < 0.01$). Similarly, there was a significant decrease in the serum levels of both IGF-I (Fig. 2B) and IGF-II (Fig. 2C) in BCAA-supplemented mice compared with the CRF-1 – fed ($P < 0.001$ for each comparison) and casein-supplemented mice ($P < 0.001$ and $P < 0.01$, respectively).

Effects of BCAA supplementation on the expression levels of IGF-IR, p-IGF-IR, p-GSK-3β, p-Akt, and COX-2 proteins, and on cell proliferative activity in the colonic mucosa of AOM-treated db/db *mice.* Hyperinsulinemia and abnormal activation of the IGF/IGF-IR axis play a critical role in obesity-related CRC development (3, 6 – 10). Therefore, the effects of BCAA on the levels of IGF-IR and the phosphorylated (i.e., activated) form of IGF-IR proteins, and cell proliferation were examined in the colonic mucosa of AOM-treated mice. As shown in Fig. 2D, western blot analyses showed that BCAA supplementation caused a decrease in the levels of IGF-IR ($P < 0.001$ for each comparison) and p-IGF-1R ($P < 0.001$ for each comparison) proteins compared with the CRF-1 – fed and casein-supplemented mice. Supplementation with BCAA also decreased the expression levels of the phosphorylated (i.e., inactivated) form of GSK-3β ($P < 0.01$ for each comparison), the phosphorylated (i.e., activated) form of Akt ($P < 0.001$ for each comparison), and COX-2 ($P < 0.01$ for each comparison) proteins compared with the control groups. The finding that BCAA supplementation inhibited the phosphorylation of Akt is considered to be significant because the activation of this protein is one of the critical targets in the constitutive activation of the IGF/IGF-IR axis in colorectal carcinogenesis (30).

In addition, as shown in Fig. 3, the PCNA labeling index of nonlesional crypts in the BCAA-supplemented mice was significantly smaller than that of the CRF-1 – fed and casein-supplemented mice ($P < 0.001$ for each comparison), thus indicating that BCAA supplementation significantly inhibits cell proliferation in the colonic mucosa of the AOM-treated *db/db* mice.

Discussion

The present study clearly indicated that dietary supplementation with BCAA effectively suppressed the development of putative precursor lesions, ACF and BCAC (Fig. 1), for CRC

DOI:10.1158/1078-0432.CCR-08-2093

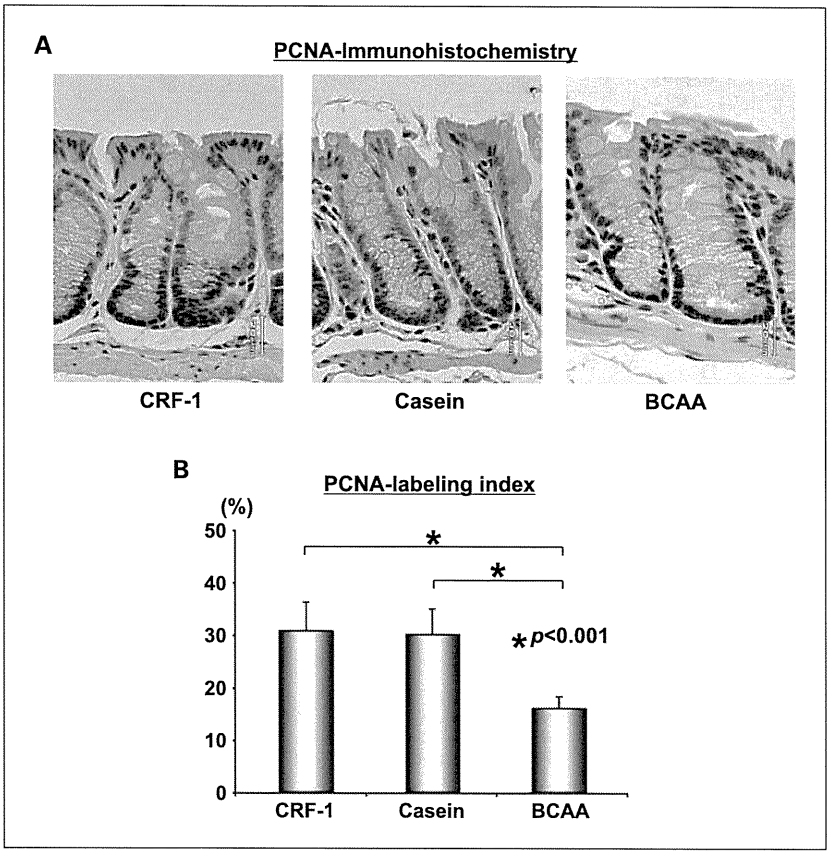

Fig. 3. The effect of BCAA supplementation on colonic epithelial cell proliferation in AOM-treated *db/db* mice. *A,* immunohistochemical staining of the normal crypts in the colon of AOM-treated *db/db* mice with anti-PCNA antibody. Sections of the colon were analyzed from CRF-1 – fed, casein-supplemented, and BCAA-supplemented mice, respectively. They were stained with anti-PCNA monoclonal antibody as described in Materials and Methods. Representative photographs from each group are shown. Bar, 20 μm. *B,* PCNA labeling index in the normal crypts in the colon of AOM-treated *db/db* mice. *Bars,* SD of triplicate assays.

(Table 2) by improving hyperlipidemia and hyperleptinemia in *db/db* mice (Table 3). The suppressive effect of BCAA in the early phase of obesity-related colorectal carcinogenesis was also associated, most likely, with the improvement of hyperinsulinemia (Fig. 2A) and the inhibition of cell proliferation on the colonic mucosa of experimental mice (Fig. 3). BCAA supplementation has also been reported to significantly decrease the incidence of hepatocellular carcinoma in patients with chronic liver disease if they had a body mass index score ≥25, and this effect might be associated with improvement of insulin resistance (15, 16, 31). Thus, BCAA might effectively prevent cancer development, at least in several organs, in obese subjects who are considered to have insulin resistance syndrome (3).

How can BCAA exert chemopreventive effects on obesity-related colorectal carcinogenesis? As described above, insulin resistance might be a critical target of BCAA in this beneficial effect because insulin has oncogenic properties on CRC cells. For instance, insulin stimulates the proliferation of CRC cells and promotes colorectal tumor growth in animal models (6–8). These reports, therefore, suggest that BCAA inhibits the development of colonic premalignant lesions (Table 2) and excessive cell proliferation in the colonic mucosa of AOM-injected *db/db* mice (Fig. 3) by improving insulin resistance (Fig. 2A). Recent studies by others have indicated that BCAA improves glucose tolerance by modulating insulin-independent glucose uptake into skeletal muscle in rodent models (32, 33). An improvement of insulin resistance and glucose tolerance by BCAA has also been shown by certain clinical trials (15, 31).

In addition, it is widely accepted that insulin resistance causes alterations in the IGF/IGF-IR axis, which may be closely associated with the development of CRC (9, 10, 30). For instance, the IGF-IR protein is overexpressed in BCAC compared with the surrounding normal cryptal cells (11). Therefore, the IGF/IGF-IR system is regarded as one of the effective targets with respect to the prevention of CRC (11). Our observations described herein comprise the first report showing that BCAA decreases the serum levels of IGF-I and IGF-II (Fig. 2B and C), thereby inhibiting the expression and activation of IGF-IR on the colonic mucosa of AOM-treated *db/db* mice (Fig. 2D). Our findings suggest that not only the improvement of insulin resistance but the inhibition of IGF/IGF-IR activation by BCAA plays a critical role in suppressing obesity-related and diabetes mellitus–related colorectal carcinogenesis.

The present study revealed that BCAA supplementation in the diet prevents the development of BCAC (Table 2), which is characterized by abundant β-catenin protein expression (23) and also accumulates the IGF-IR protein (11) while decreasing the expression levels of p-Akt and p-GSK-3β proteins on the colonic mucosa of AOM-treated *db/db* mice (Fig. 2D). Recent *in vitro* studies have indicated that insulin and the IGF/IGF-IR axis stabilize and activate the Wnt/β-catenin pathway, which is involved in the development of CRC (34, 35). GSK-3β, which can be phosphorylated by phosphatidylinositol 3-kinase/Akt via insulin or IGF treatment, is considered to be a key kinase for CRC development because the inactivation of GSK-3β leads to the dissociation of the adenomatous polyposis coli/axin/β-catenin complex and cytosolic β-catenin accumulation (36).

DOI:10.1158/1078-0432.CCR-08-2093

Free accumulated β-catenin translocates into the nucleus and forms a complex with the transcription factor T cell factor, thereby activating the transcription of target genes, including cyclin D1 and c-Myc, and thus contributing to abnormal proliferation and tumor progression (37, 38). Therefore, supplementation with BCAA, which targets insulin-associated and IGF-associated β-catenin accumulation by decreasing the levels of p-Akt and p-GSK-3β proteins (Fig. 2D), might be an effective strategy to prevent the development of CRC.

In addition to the beneficial effects mentioned above, BCAA has other physiologic activities that might be useful to prevent the development of CRC. For instance, supplementation with BCAA is capable of reducing the production of oxidative stress and microinflammation in patients with liver cirrhosis, which possibly leads to a decrease in the occurrence of hepatocellular carcinoma (39). In the current study, BCAA caused a decrease in the expression of the COX-2 protein in the colonic mucosa of AOM-treated *db/db* mice (Fig. 2D). COX-2 is one of the main mediators in the inflammatory signaling pathway and is certainly involved in CRC development; therefore, it might be a critical target for CRC chemoprevention (40). This effect might be explained by the inhibitory effect of BCAA on the IGF/IGF-IR axis because the activation of this axis mediates COX-2 expression (41, 42). Additional studies are required to clarify the direct effects of BCAA on inflammation and their relevance to the antitumor effects of this agent.

In summary, the prevention of CRC by targeting the dysregulation of energy homeostasis, especially insulin resistance and the activation of the IGF/IGF-IR axis, might be a promising strategy for obese people who are at an increased risk of CRC. BCAA seems to be a potentially effective and critical candidate for this purpose because this agent can improve insulin resistance while also exerting a depressant effect on the IGF/IGF-IR axis. The current findings, as well as those from a previous report (11), also suggest the possibility of using specific agents that target insulin resistance as chemopreventive agents for other obesity-related and diabetes mellitus–related malignancies. Therefore, insulin resistance–improving agents, including BCAA, are worthy of being further investigated as candidates for novel chemopreventive agents that may find a potential role in the society today, in which excessive body weight has been found to be associated with the risk of various types of human epithelial malignancies (43, 44).

Disclosure of Potential Conflicts of Interest

No potential conflicts of interest were disclosed.

Acknowledgments

We thank Yukari Nomura for her excellent technical assistance.

References

1. Giovannucci E, Michaud D. The role of obesity and related metabolic disturbances in cancers of the colon, prostate, and pancreas. Gastroenterology 2007;132:2208–25.
2. Frezza EE, Wachtel MS, Chiriva-Internati M. Influence of obesity on the risk of developing colon cancer. Gut 2006;55:285–91.
3. Chang CK, Ulrich CM. Hyperinsulinaemia and hyperglycaemia: possible risk factors of colorectal cancer among diabetic patients. Diabetologia 2003;46:595–607.
4. Berster JM, Goke B. Type 2 diabetes mellitus as risk factor for colorectal cancer. Arch Physiol Biochem 2008;114:84–98.
5. Yang YX, Hennessy S, Lewis JD. Insulin therapy and colorectal cancer risk among type 2 diabetes mellitus patients. Gastroenterology 2004;127:1044–50.
6. Bjork J, Nilsson J, Hultcrantz R, Johansson C. Growth-regulatory effects of sensory neuropeptides, epidermal growth factor, insulin, and somatostatin on the non-transformed intestinal epithelial cell line IEC-6 and the colon cancer cell line HT 29. Scand J Gastroenterol 1993;28:879–84.
7. Corpet DE, Jacquinet C, Peiffer G, Tache S. Insulin injections promote the growth of aberrant crypt foci in the colon of rats. Nutr Cancer 1997;27:316–20.
8. Tran TT, Medline A, Bruce WR. Insulin promotion of colon tumors in rats. Cancer Epidemiol Biomarkers Prev 1996;5:1013–5.
9. Singh P, Rubin N. Insulin-like growth factors and binding proteins in colon cancer. Gastroenterology 1993;105:1218–37.
10. Durai R, Yang W, Gupta S, Seifalian AM, Winslet MC. The role of the insulin-like growth factor system in colorectal cancer: review of current knowledge. Int J Colorectal Dis 2005;20:203–20.
11. Shimizu M, Shirakami Y, Sakai H, et al. EGCG suppresses azoxymethane-induced colonic premalignant lesions in male C57BL/KsJ-db/db mice. Cancer Prev Res 2008;1:298–304.
12. Moriwaki H, Miwa Y, Tajika M, Kato M, Fukushima H, Shiraki M. Branched-chain amino acids as a protein- and energy-source in liver cirrhosis. Biochem Biophys Res Commun 2004;313:405–9.
13. Marchesini G, Bianchi G, Merli M, et al. Nutritional supplementation with branched-chain amino acids in advanced cirrhosis: a double-blind, randomized trial. Gastroenterology 2003;124:1792–801.
14. Muto Y, Sato S, Watanabe A, et al. Effects of oral branched-chain amino acid granules on event-free survival in patients with liver cirrhosis. Clin Gastroenterol Hepatol 2005;3:705–13.
15. Kawaguchi T, Nagao Y, Matsuoka H, Ide T, Sata M. Branched-chain amino acid-enriched supplementation improves insulin resistance in patients with chronic liver disease. Int J Mol Med 2008;22:105–12.
16. Muto Y, Sato S, Watanabe A, et al. Overweight and obesity increase the risk for liver cancer in patients with liver cirrhosis and long-term oral supplementation with branched-chain amino acid granules inhibits liver carcinogenesis in heavier patients with liver cirrhosis. Hepatol Res 2006;35:204–14.
17. El-Serag HB, Rudolph KL. Hepatocellular carcinoma: epidemiology and molecular carcinogenesis. Gastroenterology 2007;132:2557–76.
18. Davila JA, Morgan RO, Shaib Y, McGlynn KA, El-Serag HB. Diabetes increases the risk of hepatocellular carcinoma in the United States: a population based case control study. Gut 2005;54:533–9.
19. Hirose Y, Hata K, Kuno T, et al. Enhancement of development of azoxymethane-induced colonic premalignant lesions in C57BL/KsJ-db/db mice. Carcinogenesis 2004;25:821–5.
20. Suzuki R, Kohno H, Yasui Y, et al. Diet supplemented with citrus unshiu segment membrane suppresses chemically induced colonic preneoplastic lesions and fatty liver in male db/db mice. Int J Cancer 2007;120:252–8.
21. Hayashi K, Suzuki R, Miyamoto S, et al. Citrus auraptene suppresses azoxymethane-induced colonic preneoplastic lesions in C57BL/KsJ-db/db mice. Nutr Cancer 2007;58:75–84.
22. Bird RP, Good CK. The significance of aberrant crypt foci in understanding the pathogenesis of colon cancer. Toxicol Lett 2000;112–113:395–402.
23. Yamada Y, Mori H. Pre-cancerous lesions for colorectal cancers in rodents: a new concept. Carcinogenesis 2003;24:1015–9.
24. Zhang Y, Guo K, LeBlanc RE, Loh D, Schwartz GJ, Yu YH. Increasing dietary leucine intake reduces diet-induced obesity and improves glucose and cholesterol metabolism in mice via multimechanisms. Diabetes 2007;56:1647–54.
25. Hata K, Tanaka T, Kohno H, et al. β-Catenin-accumulated crypts in the colonic mucosa of juvenile ApcMin/+ mice. Cancer Lett 2006;239:123–8.
26. Mori H, Yamada Y, Kuno T, Hirose Y. Aberrant crypt foci and β-catenin accumulated crypts; significance and roles for colorectal carcinogenesis. Mutat Res 2004;566:191–208.
27. Shirakami Y, Shimizu M, Tsurumi H, Hara Y, Tanaka T, Moriwaki H. EGCG and Polyphenon E attenuate inflammation-related mouse colon carcinogenesis induced by AOM and DSS. Mol Med Rep 2008;1:355–61.
28. Shimizu M, Shirakami Y, Sakai H, et al. EGCG inhibits activation of the insulin-like growth factor (IGF)/IGF-1 receptor axis in human hepatocellular carcinoma cells. Cancer Lett 2008;262:10–8.
29. Shiraki M, Shimomura Y, Miwa Y, et al. Activation of hepatic branched-chain α-keto acid dehydrogenase complex by tumor necrosis factor-α in rats. Biochem Biophys Res Commun 2005;328:973–8.
30. Adachi Y, Lee CT, Coffee K, et al. Effects of genetic blockade of the insulin-like growth factor receptor in human colon cancer cell lines. Gastroenterology 2002;123:1191–204.
31. Urata Y, Okita K, Korenaga K, Uchida K, Yamasaki T, Sakaida I. The effect of supplementation with branched-chain amino acids in patients with liver cirrhosis. Hepatol Res 2007;37:510–6.
32. Nishitani S, Takehana K, Fujitani S, Sonaka I. Branched-chain amino acids improve glucose metabolism in rats with liver cirrhosis. Am J Physiol Gastrointest Liver Physiol 2005;288:G1292–300.

DOI:10.1158/1078-0432.CCR-08-2093

33. Nishitani S,Takehana K. Pharmacological activities of branched-chain amino acids: augmentation of albumin synthesis in liver and improvement of glucose metabolism in skeletal muscle. Hepatol Res 2004;30S:19–24.

34. Sun J, Jin T. Both Wnt and mTOR signaling pathways are involved in insulin-stimulated proto-oncogene expression in intestinal cells. Cell Signal 2008; 20:219–29.

35. Playford MP, Bicknell D, Bodmer WF, Macaulay VM. Insulin-like growth factor 1 regulates the location, stability, and transcriptional activity of β-catenin. Proc Natl Acad Sci U S A 2000;97:12103–8.

36. Papkoff J, Aikawa M. WNT-1 and HGF regulate GSK3 β activity and β-catenin signaling in mammary epithelial cells. Biochem Biophys Res Commun 1998; 247:851–8.

37. Tetsu O, McCormick F. β-catenin regulates expression of cyclin D1 in colon carcinoma cells. Nature 1999; 398:422–6.

38. He TC, Sparks AB, Rago C, et al. Identification of c-MYC as a target of the APC pathway. Science 1998; 281:1509–12.

39. Ohno T, Tanaka Y, Sugauchi F, et al. Suppressive effect of oral administration of branched-chain amino acid granules on oxidative stress and inflammation in HCV-positive patients with liver cirrhosis. Hepatol Res 2008;38:683–8.

40. Gupta RA, Dubois RN. Colorectal cancer prevention and treatment by inhibition of cyclooxygenase-2. Nat Rev Cancer 2001;1:11–21.

41. Di Popolo A, Memoli A, Apicella A, et al. IGF-II/IGF-I receptor pathway up-regulates COX-2 mRNA expression and PGE2 synthesis in Caco-2 human colon carcinoma cells. Oncogene 2000;19:5517–24.

42. Stoeltzing O, Liu W, Fan F, et al. Regulation of cyclooxygenase-2 (COX-2) expression in human pancreatic carcinoma cells by the insulin-like growth factor-I receptor (IGF-IR) system. Cancer Lett 2007;258: 291–300.

43. Renehan AG, Tyson M, Egger M, Heller RF, Zwahlen M. Body-mass index and incidence of cancer: a systematic review and meta-analysis of prospective observational studies. Lancet 2008;371:569–78.

44. Wiseman M. The Second World Cancer Research Fund/American Institute for Cancer Research Expert Report. Food, nutrition, physical activity, and the prevention of cancer: a global perspective. Proc Nutr Soc 2008:1–4.

Carcinogenesis vol.30 no.9 pp.1544–1552, 2009
doi:10.1093/carcin/bgp166
Advance Access publication July 3, 2009

(−)-Epigallocatechin gallate downregulates EGF receptor via phosphorylation at Ser1046/1047 by p38 MAPK in colon cancer cells

Seiji Adachi[1,2], Masahito Shimizu[1], Yohei Shirakami[1], Junichi Yamauchi[2], Hideo Natsume[2], Rie Matsushima-Nishiwaki[2], Satoshi To[3], I.Bernard Weinstein[3], Hisataka Moriwaki[1] and Osamu Kozawa[2,*]

[1]Department of Gastroenterology and [2]Department of Pharmacology, Gifu University Graduate School of Medicine, Gifu 501-1194, Japan and [3]Herbert Irving Comprehensive Cancer Center, Columbia University, Medical Center, NY 10032, USA

*To whom correspondence should be addressed. Tel: +81 58 230 6214; Fax: +81 58 230 6215;
Email: okozawa@gifu-u.ac.jp

We previously reported that (−)-epigallocatechin gallate (EGCG) in green tea alters plasma membrane organization and causes internalization of epidermal growth factor receptor (EGFR), resulting in the suppression of colon cancer cell growth. In the present study, we investigated the detailed mechanism underlying EGCG-induced downregulation of EGFR in SW480 colon cancer cells. Prolonged exposure to EGCG caused EGFR degradation. However, EGCG required neither an ubiquitin ligase (c-Cbl) binding to EGFR nor a phosphorylation of EGFR at tyrosine residues, both of which are reportedly necessary for EGFR degradation induced by epidermal growth factor. In addition, EGCG induced phosphorylation of p38 mitogen-activated protein kinase (MAPK), a stress-inducible kinase believed to negatively regulate tumorigenesis, and the inhibition of p38 MAPK by SB203580, a specific p38 MAPK inhibitor, or the gene silencing using p38 MAPK-small interfering RNA (siRNA) suppressed the internalization and subsequent degradation of EGFR induced by EGCG. EGFR underwent a gel mobility shift upon treatment with EGCG and this was canceled by SB203580, indicating that EGCG causes EGFR phosphorylation via p38 MAPK. Moreover, EGCG caused phosphorylation of EGFR at Ser1046/1047, a site that is critical for its downregulation and this was also suppressed by SB203580 or siRNA of p38 MAPK. Taken together, our results strongly suggest that phosphorylation of EGFR at serine 1046/1047 via activation of p38 MAPK plays a pivotal role in EGCG-induced downregulation of EGFR in colon cancer cells.

Introduction

Colon cancer is the second leading cause of cancer-related mortality in Western countries. Members of the epidermal growth factor receptor (EGFR) family, which are frequently overexpressed in several types of human cancers, including cancers of the lung (1), head and neck (2), prostate (3), breast (4), pancreas (5) and colon (6), have been associated with abnormal growth of these tumors. Binding of ligand to EGFR leads to receptor dimerization, autophosphorylation and activation of several downstream signaling pathways, which upon activation lead to cell proliferation, motility and enhanced survival (7). There are several mechanisms by which EGFR becomes oncogenic, including (i) increased EGFR levels; (ii) autocrine and/or paracrine growth factor loops; (iii) heterodimerization with other EGFR family members and cross talk with heterologous receptor systems; (iv) defective receptor downregulation (described below in detail) and (v) activating mutations (8). In cohort studies, EGFR overexpression has been associated with chemoresistance, disease progression and poor survival (9). In clinical trials, increasing evidence shows the efficacy of EGFR-targeted agents, including monoclonal antibodies on the one hand and tyrosine kinase inhibitors on the other (10). In addition, ongoing clinical trials continue to investigate EGFR therapeutics in various treatment settings (7,10).

Receptor downregulation is the most prominent regulator of EGFR signal attenuation and involves the internalization and subsequent degradation of the activated receptor in the lysosomes (8). Some agents that induce ligand-independent internalization and degradation of EGFR, such as the 225 mouse antibody (11) and gemcitabine (5) could have promising potential for cancer therapies (12). In contrast, the other factors or agents, such as oxidative stress (13), ultraviolet (UV) irradiation (14) and cisplatin (15), can induce internalization of the EGFR, but not degradation. They differ in their effects on the fate of the receptors, downstream signaling and cell proliferation.

With the current knowledge of the mechanism underlying EGFR downregulation, this molecular event seems to involve several important phosphorylation sites. One is the phosphorylation at tyrosine (Tyr) 1045, which provides a docking site for the ubiquitin ligase c-Cbl resulting in ubiquitination of the EGFR (16). The others are the phosphorylation at serine or threonine residues, which is thought to represent a mechanism for attenuation of the receptor kinase activity (17–19). Among the major sites of serine and threonine phosphorylation of the EGFR, it has previously been shown that serine 1046/1047 (Ser1046/7) phosphorylation site is required for EGFR desensitization in epidermal growth factor (EGF)-treated cells (19). Moreover, mutations of Ser1046/7 are reported to cause a marked inhibition of the EGF-stimulated endocytosis and downregulation of cell surface receptors (18). However, the regulatory mechanism behind EGFR phosphorylation at Ser1046/7 remains to be clarified.

There is an evidence that cisplatin induces EGFR internalization, which is mediated by p38 mitogen-activated protein kinase (MAPK)-dependent phosphorylation of the receptor on threonine 669 (15). Gemcitabine also induces EGFR internalization and subsequent degradation that may be a novel mechanism for gemcitabine-mediated cell death (5). In addition, recent reports show that the activation of p38 MAPK is necessary for gemcitabine-induced cytotoxicity (20,21). Therefore, it is of interest to investigate the effect of anticancer drug on p38 MAPK since this signaling pathway is implicated in suppression of tumorigenesis (22,23).

(−)-Epigallocatechin gallate (EGCG) is the major biologically active polyphenol in green tea; it has been shown to inhibit the growth of several types of cancer cell lines via suppression of phosphorylation (i.e. activation) of the EGFR and inhibition of several downstream signaling pathways (2,4,6,24). We previously reported that the inhibitory effect of EGCG on EGF binding to the EGFR or EGFR dimerization is associated with alterations in lipid organization in the plasma membrane (lipid rafts) of colon cancer cells (25). Since lipid rafts are thought to play an important role in endocytosis, it is most likely that the alteration of lipid rafts induced by EGCG is associated with the cellular localization of the EGFR. Moreover, we have recently reported that EGCG can induce internalization of EGFR into endosomes, which can recycle back to the cell surface (26).

In the present study, we investigated the mechanism underlying EGCG-induced EGFR internalization in colon cancer cells because we suggest that this internalization of EGFR would explain, at least in part, the mechanism of anticancer effect of

Abbreviations: EGCG, (−)-epigallocatechin gallate; EGF, epidermal growth factor; EGFR, epidermal growth factor receptor; MAPK, mitogen-activated protein kinase; siRNA, small interfering RNA; UV, ultraviolet.

© The Author 2009. Published by Oxford University Press. All rights reserved. For Permissions, please email: journals.permissions@oxfordjournals.org

EGCG and other related compounds (26). Interestingly, we observed that the inhibition of p38 MAPK abolished the EGCG-induced internalization and subsequent degradation of EGFR, suggesting that this MAPK plays an important role in the change of EGFR trafficking. Furthermore, EGCG induced phosphorylation of EGFR at Ser1046/7 via p38 MAPK, indicating that this phosphorylation plays a pivotal role in EGFR downregulation induced by EGCG.

Materials and methods

Cell culture and chemicals

SW480 human colon cancer cells were grown in Dulbecco's modified Eagle's medium (Invitrogen, San Diego, CA) containing 10% fetal calf serum and after 24 h they were incubated in serum-free medium for an additional 24 h as described previously (26). EGCG was kindly provided by Dr Yukihiko Hara (Mitsui Norin Co., Shizuoka, Japan) and was solubilized in dimethyl sulfoxide. SB203580, AG1478 and PD153035 were purchased from Calbiochem–Novabiochem Co. (La Jolla, CA). EGF and cisplatin were from Sigma Chemical Co. (St Louis, MO).

Western blotting and immunoprecipitation assay

The cells were lysed in lysis buffer [20 mM Tris (pH 7.5), 150 mM NaCl, 1 mM ethylenediaminetetraacetic acid, 1 mM ethylene glycol tetraacetic acid, 1% Triton X-100, 2.5 mM sodium pyrophosphate, 50 mM NaF, 50 mM *N*-2-hydroxyethylpiperazine-*N'*-2-ethanesulfonic acid, 1 mM Na_3VO_4 and 2 mM phenylmethylsulfonyl fluoride] and scraped from the Petri dishes. Protein extracts were then examined by western blot analysis as described previously (26). The antibodies used in these studies were anti-EGFR, glyceraldehyde 3-phosphate dehydrogenase (Santa Cruz Biotechnology, Santa Cruz, CA), anti-phospho-EGFR (Ser1046/7), anti-phospho-EGFR (Tyr1045), anti-c-Cbl, anti-pan-phospho-threonine (42H4), anti-phospho-p38 MAPK, anti-p38 MAPK (Cell Signaling, Beverly, MA) and anti β-actin (Sigma). Anti-mouse IgG or anti-rabbit IgG antibodies (Amersham Pharmacia Biotech, Buckinghamshire, UK) were used as the secondary antibodies. Each membrane was developed using an enhanced chemiluminescence detection system (Amersham Pharmacia Biotech). For detection of immunoprecipitated EGFR, cell lysates (500 μg each) were incubated for 12 h at 4°C with an anti-EGFR antibody (Santa Cruz Biotechnology) precoupled to anti-mouse IgG agarose beads. Protein extracts were then eluted and examined by western blotting using the indicated antibodies.

Gel mobility shift assays

Sodium dodecyl sulfate–polyacrylamide gel electrophoresis was performed in 4% polyacrylamide large gel for 6 h at 4°C to separate proteins clearly.

Small interfering RNA protocol

Predesigned small interfering RNAs (siRNAs) targeting p38 MAPK (On-TARGET plus Duplex J-003512-20, Human MAPK14) was purchased from Thermo Fisher Scientific K.K. (Yokohama, Japan). Sequences are as follows: sense, 5′-GGAAUUCAAUGAUGUGUAUUU-3′ and antisense, 5′-AUACACAUCAUUGAAUUCCUU-3′. Transfection was performed according to the manufacturer's protocol (Bio-Rad, Tokyo, Japan). In brief, 2.5 μl of siLentFect (Bio-Rad) and finally 100 nM of siRNA were diluted with fetal calf serum-free Dulbecco's modified Eagle's medium, preincubated at room temperature for 20 min and then added to the culture medium containing 10% fetal calf serum. Cells were incubated at 37°C for 48 h with siRNA–siLentFect complexes and subsequently harvested for preparation of western blot analysis.

Immunofluorescence microscopy studies

Immunofluorescence microscopy studies were performed as described previously (26). Live cells grown on coverslip-bottom dishes were first exposed to the mouse anti-EGFR antibody that recognizes the extracellular domain of EGFR and then treated with EGF (100 ng/ml) or EGCG (50 μM) for 30 min at 37°C, followed by fixation with 3% paraformaldehyde for 10 min on ice. They were then exposed to 0.1% Triton X-100 for 10 min to permeabilize the cell membrane, followed by exposure to Alexa Fluor 488®-conjugated goat anti-mouse IgG antibody for 1 h for EGFR (green signal). In some cases, the fixed cells were exposed to an anti-c-Cbl antibody, followed by exposure to Alexa Fluor 488®-conjugated goat anti-rabbit IgG antibody for c-Cbl (green signal) and Alexa Fluor 546®-conjugated goat anti-mouse IgG for EGFR (red signal) for 1 h. Finally, they were exposed to 4′,6-diamidino-2-phenylindole (Wako, Tokyo, Japan) for 20 min and the cells were then examined by fluorescence microscopy, BIOREVO (BZ-9000) (Keyence, Tokyo, Japan) according to the manufacturer's protocol.

Quantification of cell surface EGFR by enzyme-linked immunosorbent assay

Quantification of cell surface EGFR was performed as described previously (26). In brief, SW480 cells were pretreated with the indicated compounds and then exposed to the mouse anti-EGFR antibody (Santa Cruz Biotechnology) that recognizes the extracellular domain of the EGFR (1:50 dilution), in Dulbecco's modified Eagle's medium containing 1% bovine serum albumin for 15 min at 37°C. The cells were then treated with EGCG (25 μM) for 30 min at 37°C and then fixed with 4% paraformaldehyde for 10 min on ice. After blocking with 1% bovine serum albumin in phosphate-buffered saline for 1 h, the cells were exposed to an anti-mouse IgG, horseradish peroxidase-linked whole antibody (GE Healthcare, Piscataway, NJ) for 1 h at room temperature, followed by washing four times with phosphate-buffered saline containing 1% bovine serum albumin. Finally, the cells were exposed to 50 μl of 1-step™ Ultra TMB-ELISA reagent (Pierce, Rockford, IL) for 5 min at room temperature. Fifty microliters of 2 M sulfuric acid was then added to each well to stop the reaction. The absorbance of each sample at 450 nm was then measured.

Results

Continuous treatment with EGCG caused degradation of the EGFR in SW480 colon cancer cells

Since EGCG induces apoptosis of colon cancer cells (6), it is of interest to examine the effect of longer exposure to EGCG on these cells that highly express EGFR proteins. We first measured the levels of EGFR in the presence or absence of EGCG by western blot analysis (Figure 1). We examined the effect of various doses of EGCG on the levels of EGFR and found that exposure to 25 μM of EGCG for 24 h significantly induced degradation of EGFR (Figure 1A, lane 4) and that 50 μM of EGCG almost completely degraded them (Figure 1A, lane 5). We next performed a time course experiment and found that treatment with EGCG (50 μM) for 8 h caused partial degradation of the EGFR (Figure 1B, lane 5) and that treatment with EGCG for 12 h caused marked degradation of EGFR (Figure 1B, lane 6). Although we recently reported that transient exposure to EGCG induced internalization of cell surface-associated EGFR into endosomes, which could recycle back to the cell surface (26), this was not seen in this study because in the previous study we examined the effect of continuous, not transient, treatment with EGCG. We also performed cell counting assay using 3-[4,5-dimethylthiazol-2-yl]-2,5-diphenyltetrazolium bromide and found that EGCG did not influence cell number of SW480 within 24 h (data not shown), whereas decrease in the level of EGFR were observed within 12 h (Figure 1B).

The degradation of EGFR induced by EGCG is not associated with c-Cbl in SW480 colon cancer cells

It is well known that c-Cbl, an ubiquitin E3 ligase, plays a role in downregulation of EGFR (16,27,28). Thus, c-Cbl was shown to ubiquitylate and downregulate EGFR (29) and was formally established as a RING finger-type E3 ubiquitin ligase (30,31). Therefore, we next examined the correlation between EGFR and c-Cbl in the EGCG-induced EGFR downregulation. We first found in immunofluorescence microscope studies that EGCG as well as EGF induced internalization of EGFR (Figure 2A, panels 2 and 3), which is consistent with our previous studies (26). We next performed colocalization assays of these internalized EGFRs (panels 1–3) and c-Cbl (panels 4–6) and found that internalized EGFR induced by EGCG did not colocalize with the c-Cbl protein (panel 12), whereas the internalized EGFR induced by EGF were clearly colocalized with c-Cbl (panel 11). Many reports demonstrate that activation of EGFR induces its autophosphorylation followed by binding of c-Cbl to the Tyr1045 residue of EGFR (29). In addition, we have shown that EGCG does not cause phosphorylation of EGFR at any tyrosine residues and that the internalized EGFRs induced by EGCG are not phosphorylated at Tyr1045 residue (26). Therefore, it seems unlikely that the internalization of EGFR induced by EGCG is associated with c-Cbl.

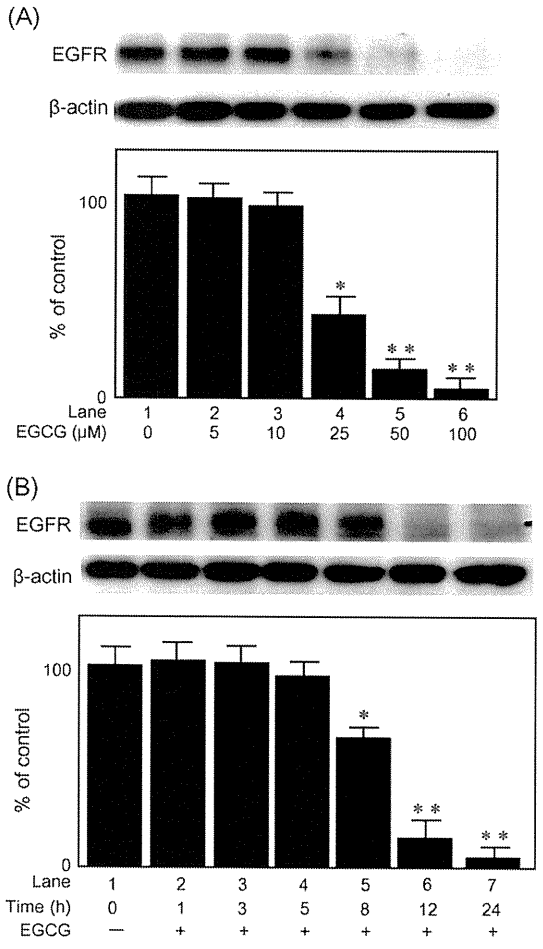

Fig. 1. Prolonged exposure to EGCG caused degradation of the EGFR. SW480 colon cancer cells were treated with the indicated doses of EGCG for 24 h (**A**) or with 50 μM of EGCG for the indicated times (**B**). Protein extracts were then prepared and examined by western blotting using anti-EGFR antibody. An antibody to β-actin was used to control for protein loading. The lower bar graph shows the quantification data for total EGFR level obtained from western blot analysis after normalization with respect to β-actin. The asterisks indicate significant decrease ($^{*}P < 0.05$ and $^{**}P < 0.01$, respectively) in comparison with the control (lane 1).

To further confirm the above results, we next performed binding assays of EGFR and c-Cbl using immunoprecipitation–western blot analysis. As shown in Figure 2B, EGF caused the interaction of EGFR with c-Cbl (lane 3), whereas EGCG failed to induce their interaction (lane 4). Because both EGF and EGCG did not influence the expression level of c-Cbl (Figure 2B, middle panel), it is probable that EGCG induces internalization of EGFR independently of c-Cbl.

Phosphorylation of EGFR at tyrosine residues is not necessary for its internalization or degradation induced by EGCG in SW480 colon cancer cells

As described above, it is well known that EGF causes phosphorylation of EGFR at Tyr1045, the major docking site for the ubiquitin ligase c-Cbl (16). Therefore, we next investigated whether or not this phosphorylation is required for the degradation induced by EGCG. We first examined the effects of AG1478 and PD153035, both of which are EGFR-specific tyrosine kinase inhibitors (32,33), on the internalization of EGFR induced by EGCG in immunofluorescence microscope studies. We first confirmed that either 2 μM of AG1478 or 10 μM of PD153035 significantly blocked EGF-induced phosphorylation of EGFR at tyrosine residues (Figure 3A, lanes 4 and 6 compared with lane 2). In the presence of AG1478 or PD153035, the internalization of EGFR induced by EGCG was not suppressed (Figure 3B, upper panels 4 and 6 compared with panel 2). In addition, quantification analysis by enzyme-linked immunosorbent assay showed no effect in cell surface amount of EGFR by the inhibition of tyrosine kinase on EGFR (Figure 3B, lower bar graphs, lanes 4 and 6 compared with lane 2). Moreover, we found that EGFR was degraded by EGCG even in the presence of either AG1478 or PD153035 (Figure 3C and D, lane 4 compared with lane 2, respectively). Therefore, it seems unlikely that phosphorylation of EGFR at any tyrosine residues is necessary for the internalization or degradation of EGFR induced by EGCG.

EGCG induced phosphorylation of p38 MAPK in SW480 colon cancer cells

It has recently been reported that cisplatin, a widely used anticancer drug, induces EGFR internalization, which is mediated by p38 MAPK-dependent phosphorylation of the receptor on threonine 669 (15). Receptor internalization induced by UV is also caused by p38 MAPK (34). Since it has been shown that p38 MAPK can negatively regulate tumorigenesis (23), we next examined the effect of EGCG on phosphorylation (i.e. activation) of p38 MAPK in SW480 cells. The upper panels in Figure 4 display representative western blotting images and the lower bar graph provides quantification of phospho-p38 MAPK after normalization with respect to total p38 MAPK, as determined by densitometry. As expected, p38 MAPK was significantly phosphorylated within 30 min by the treatment with EGCG and reached maximum effect at 1 h after the exposure (Figure 4, lower graph). These results led us to further investigate the role of activated p38 MAPK in EGCG-treated cells.

Inhibition of p38 MAPK activation suppressed downregulation of EGFR induced by EGCG in SW480 colon cancer cells

We next examined the effect of a specific inhibitor of p38 MAPK, SB203580 (35), on the internalization of EGFR induced by EGCG. We first confirmed that SB203580 truly inhibited phosphorylation (activation) of p38 MAPK in SW480 cells (Figure 5A). As we have shown previously (26), a 30 min exposure to 25 μM of EGCG caused internalization of EGFR (Figure 5B, panel 2). Quantification analysis by enzyme-linked immunosorbent assay showed ~60% decrease in cell surface amount of EGFR (Figure 5B, lower bar graph). When the cells were pretreated with SB203580 (10 μM) for 1 h and then exposed to EGCG (25 μM) for 30 min, internalization of EGFR was significantly blocked (Figure 5B, upper panel 4 and lower graph, lane 4). We next examined the effect of SB203580 on EGFR degradation induced by continuous treatment of the cells with EGCG. Pretreatment with 2.5 μM of SB203580, which alone did not affect the EGFR levels, markedly suppressed, and 5 or 10 μM of SB203580 almost completely suppressed the degradation of EGFR induced by EGCG (Figure 5C). Furthermore, we verified the involvement of p38 MAPK in EGCG-induced degradation of EGFR utilizing the gene silencing using p38 MAPK-siRNA (Figure 5D). Whereas knock down selectively decreased expression of p38 MAPK (Figure 5D, upper panel), the degradation of EGFR induced by EGCG was significantly restored in p38 MAPK-knocked down SW480 cells (Figure 5D, lower panel, lane 4 compared with lane 2). Taken together, these results provide strong evidence that p38 MAPK plays a crucial role in the downregulation of EGFR induced by EGCG.

EGCG caused phosphorylation of EGFR at Ser1046/7 and this was blocked by SB203580 in SW480 colon cancer cells

It has previously been reported that phosphorylation of EGFR on serine and threonine residues is thought to represent a mechanism

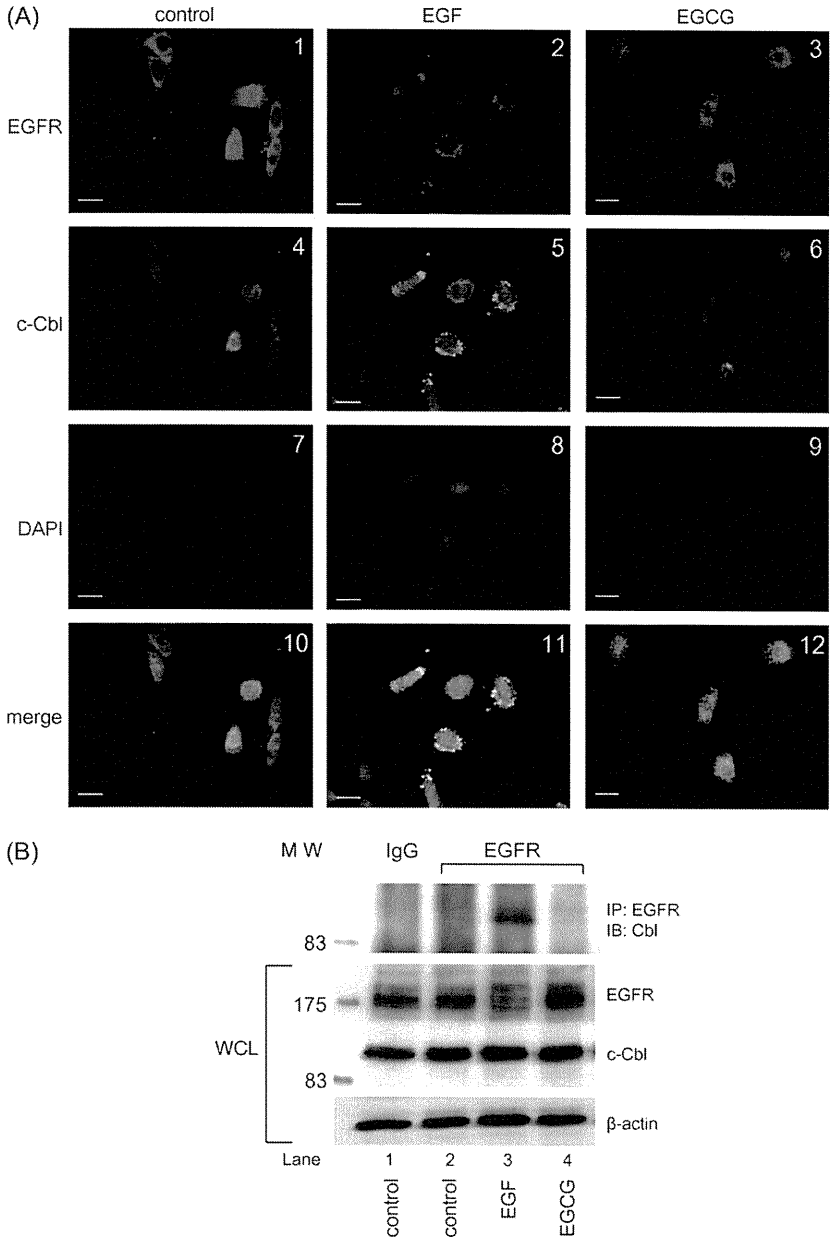

Fig. 2. The internalized EGFR induced by EGCG does not associate with c-Cbl. (**A**) SW480 cells were first labeled for 15 min at 37°C with an anti-EGFR antibody that recognizes the extracellular domain of the EGFR. They were then treated with EGF (100 ng/ml) or EGCG (25 μM) for 30 min at 37°C, followed by fixation with paraformaldehyde. After permeabilization of the cells with 0.1% Triton X-100, the cells were exposed to an anti-c-Cbl antibody (1:100 dilution) for 1 h and then treated with Alexa Fluor 546-conjugated anti-mouse secondary antibody for EGFR (red signal) and Alexa Fluor 488-conjugated anti-mouse secondary antibody for c-Cbl (green signal). After washing, the cells were exposed to 4′,6-diamidino-2-phenylindole (DAPI) (blue signal) for 20 min and then examined by fluorescence microscopy. Representative results from at least three independent experiments are shown. Scale bar indicates 20 μm. (**B**) EGF, but not EGCG, induced c-Cbl–EGFR binding. The cells were exposed to EGF (100 ng/ml) or EGCG (25 μM) for 30 min at 37°C. Then, cell lysates (500 μg each) were prepared and incubated for 12 h at 4°C with an anti-EGFR antibody precoupled to anti-mouse IgG-agarose beads. The bound protein was then analyzed by western blotting with an anti-c-Cbl antibody. The lower two panels indicate the corresponding whole-cell lysates (WCLs). MW indicates molecular weight.

for attenuation of its receptor kinase activity (17). It has also been reported that EGFR undergoes a gel mobility shift upon cisplatin treatment, which is mediated by p38 MAPK (15,34). In addition, UV induces phosphorylation of EGFR (gel mobility shift of EGFR) that was suppressed by the inhibition of activation of p38 MAPK (34). Moreover, cisplatin induces EGFR internalization that is mediated by p38 MAPK-dependent phosphorylation of the receptor on threonine 669 (15). Therefore, we examined the effect of EGCG on gel mobility shift of EGFR. First, we verified that cisplatin caused a gel mobility shift of EGFR in SW480 cells (Figure 6A, lane 4), as described in a previous study with MDA-MB-468 cells (15). Indeed, we found that EGCG had an effect similar to that of cisplatin on gel mobility shift of EGFR (Figure 6A, lane 7). The gel mobility shift of the EGFR induced by EGCG, and that induced by

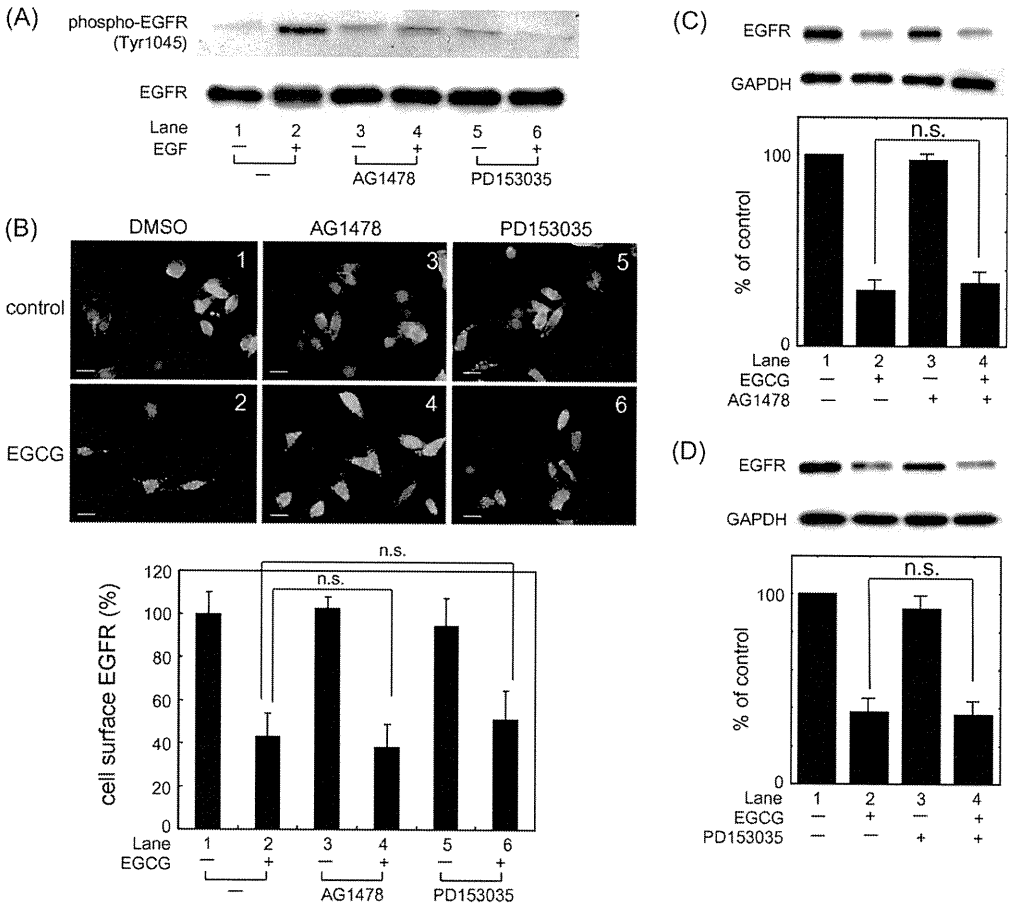

Fig. 3. EGCG-induced downregulation of EGFR does not require tyrosine phosphorylation. (**A**) SW480 cells were pretreated with vehicle, 2 μM of AG1478 or 10 μM of PD153035 for 1 h and then treated with 100 ng/ml of EGF for 15 min. Protein extracts were then harvested and examined by western blotting using antibodies against phospho-EGFR (Tyr1045) and EGFR. (**B**) SW480 cells were pretreated with vehicle, 2 μM of AG1478 or 10 μM of PD153035 for 1 h and then labeled for 15 min at 37°C with an anti-EGFR antibody that recognizes the extracellular domain of the EGFR. They were then exposed to EGCG (25 μM) for 30 min at 37°C, followed by fixation with paraformaldehyde. They were then treated with an Alexa Fluor 488-conjugated anti-mouse secondary antibody for EGFR (green signal), followed by exposure to 4′,6-diamidino-2-phenylindole (blue signal), and examined by fluorescence microscope. Representative results from at least three independent experiments are shown. Lower bar graph shows the quantification data for cell surface amount of EGFR analyzed by enzyme-linked immunosorbent assay (see details in Materials and Methods). Scale bar indicates 20 μm. (**C** and **D**) SW480 cells were pretreated with 2 μM of AG1478 (C) or 10 μM of PD153035 (D) for 1 h and then exposed to 25 μM of EGCG for 48 h. Protein extracts were then harvested and examined by western blotting using an anti-EGFR antibody. An antibody to glyceraldehyde 3-phosphate dehydrogenase (GAPDH) was used to control for protein loading. Lower bar graph shows the quantification data for the relative levels of EGFR, after normalization with respect to GAPDH, as determined by densitometry. n.s. designates no significant difference between the indicated pairs.

cisplatin, were canceled when the cells were pretreated with the specific p38 MAPK inhibitor SB203580 (Figure 6A, lanes 5, 6, 8 and 9). We next performed immunoprecipitation assays using an anti-pan-phospho-threonine antibody in order to clarify whether EGCG as well as cisplatin causes phosphorylation of EGFR at threonine residues (Figure 6B). Although we detected phosphorylation of EGFR at threonine residues when the cells were treated with cisplatin (Figure 6B, lane 2), we did not detect phosphorylation of EGFR at threonine residues when the cells were treated with EGCG (Figure 6B, lane 3). These results led us to speculate that EGCG might cause phosphorylation of EGFR at serine, rather than threonine, residues because p38 MAPK is well known to be a serine/threonine kinase (36).

It has been shown that EGFR desensitization is mediated through phosphorylation at Ser1046/7 in EGF-treated cells (19). In addition, we recently found that activation of p38 MAPK by anisomycin causes EGFR phosphorylation at Ser1046/7 (37). Therefore, we next examined the effect of EGCG on this phosphorylation and found that treatment with EGCG induced within 30 min phosphorylation of EGFR at Ser1046/7 (Figure 6C, upper panels) and that this was attenuated by pretreatment of the cells with the specific p38 MAPK inhibitor, SB203580 (Figure 6C, lower panels). Furthermore, utilizing the gene silencing using p38 MAPK-siRNA, we verified the involvement of p38 MAPK in EGCG-induced phosphorylation of EGFR at Ser1046/7 (Figure 6D) and found that the phosphorylation of EGFR at Ser1046/7 induced by EGCG was significantly suppressed in p38 MAPK-knocked down SW480 cells (Figure 6D, upper panel, lane 4 compared with lane 2). Taken together, our findings strongly suggest that EGCG causes phosphorylation of EGFR at Ser1046/7 through activation of p38 MAPK, resulting in its gel mobility shift and subsequent degradation.

Discussion

In the present study, we examined the mechanism underlying EGCG-induced downregulation of cell surface-associated EGFR in SW480 colon cancer cells because we recently reported that

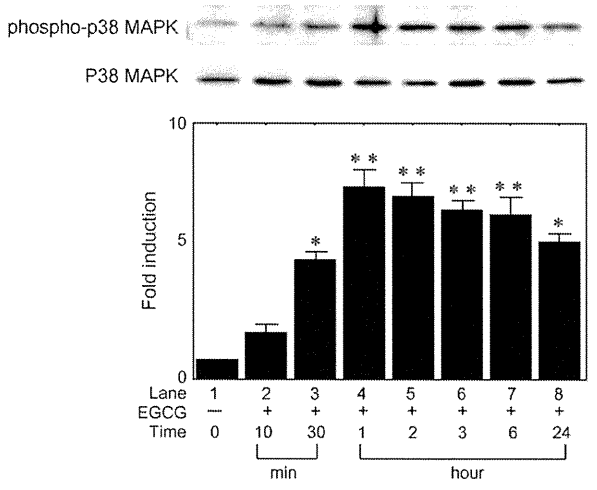

Fig. 4. EGCG causes phosphorylation of p38 MAPK within 30 min. SW480 cells were treated with 50 μM of EGCG for the indicated times and protein extracts were then harvested and examined by western blotting using anti-phospho p38 MAPK and anti-p38 MAPK antibodies. The lower bar graph shows the quantification data for the relative levels of phospho-p38 MAPK, after normalization with respect to total p38 MAPK, as determined by densitometry. The asterisks indicate significant increase ($^{*}P < 0.05$ and $^{**}P < 0.01$, respectively) as compared with the control (lane 1).

exposure of SW480 cells to relatively low concentration (20 μg/ml) of EGCG for only a brief period of time (30 min) causes EGFR internalization of the EGFR in these cells (26). In this study, we found that prolonged exposure of these cells to EGCG caused degradation of EGFR (Figure 1A). These two types of effect of EGCG are not confined to this cell type because we have obtained similar effects using another cell line, i.e HT29 colon cancer cells (data not shown). In addition, we should emphasize that in the present study we investigated the effect of continuous treatment with EGCG on EGFR, although in the previous study we examined the effect of transient exposure (for 30 min) to EGCG (26). Moreover, while it is recognized that desensitization in a broad sense includes internalization and degradation, it has previously been reported that oxidative stress induces the translocation of cell surface EGFR to perinuclei, where it is not degraded and remains active (13), and that UV induces internalization and endosome arrest of EGFR that activates MAPK kinase and MAPK (14). Since we recently reported that the internalized EGFR induced by EGCG, which is not active, fails to exert cell growth signal (26), we believe that in EGCG-treated cells both internalization and degradation of EGFR implicates desensitization and that our two studies are consistent with either interpretation.

It is well known that EGF induces EGFR autophosphorylation including Tyr1045, which is important for the binding of EGFR to the ubiquitin ligase c-Cbl. This phosphorylated EGFR is rapidly internalized and ubiquitinated by c-Cbl and then can be degraded by lysosomes (16). Since we have previously reported that EGCG causes internalization of EGFR, but not phosphorylation of EGFR at tyrosine residues including Tyr1045 (26), EGCG does not induce EGFR–c-Cbl binding (Figure 2). Therefore, the EGCG-induced degradation of EGFR seen in the present study occurs independently of c-Cbl. Furthermore, we found that EGCG induced both internalization and degradation of EGFR, even when the cells were pretreated with AG1478 or PD153035 to block phosphorylation of EGFR at tyrosine residues (Figure 3). Because the concentrations of these inhibitors we used in this study were high, we cannot exclude the possibility of their unspecific effects. However, based on our findings as a whole, it is most likely that EGCG-induced downregulation of EGFR does not require tyrosine phosphorylation. On the other hand, we found that EGCG caused phosphorylation (activation) of p38 MAPK in a time-dependent manner (Figure 4). This activation was seen within 30 min when the cells were treated with 50 μM (~22 μg/ml) of EGCG.

To investigate the involvement of p38 MAPK in internalization or degradation of EGFR induced by EGCG, we next examined the effect of a specific p38 MAPK inhibitor or the gene silencing using p38 MAPK-siRNA and found that the inhibition of p38 MAPK suppressed the internalization and subsequent degradation of EGFR induced by EGCG (Figure 5). These results strongly suggest that p38 MAPK plays a pivotal role in both the internalization and the degradation of EGFR induced by EGCG. We have seen similar effect when SW480 cells were treated with the p38 MAPK activator anisomycin (37). In the latter study, whereas EGF failed to induce activation of p38 MAPK, both p38 MAPK and stress-activated protein kinase/c-Jun N-terminal kinase were activated by anisomycin, and inhibition of p38 MAPK, but not stress-activated protein kinase/c-Jun N-terminal kinase, canceled anisomycin-induced downregulation of EGFR in SW480 colon cancer cells (37). Taken together, this evidence also supports our conclusion that EGCG-induced activation of p38 MAPK plays an important role in downregulation of EGFR.

Interestingly, our present finding that the internalized EGFR induced by EGCG did not colocalize with c-Cbl (Figure 2) is similar to the case in anisomycin-treated cells (37), indicating that downregulation of EGFR induced by EGCG as well as anisomycin does not require c-Cbl binding. In addition, we found that EGCG underwent gel mobility shift of EGFR (Figure 6A) and EGCG did not cause the phosphorylation of EGFR at threonine residues (Figure 6B), even though cisplatin caused its phosphorylation at threonine residues, which is consistent with the previous study (15). Furthermore, we demonstrated that EGCG caused the phosphorylation of EGFR at Ser1046/7, at a site that was reported to be important for degradation of EGFR (17–19,38) and that the inhibition of p38 MAPK blocked this phosphorylation (Figure 6C and D). Because gel mobility shift of EGFR induced by EGCG was also canceled when the cells were pretreated with SB203580 (Figure 6A), it is most likely that EGCG causes phosphorylation of EGFR at Ser1046/7 via activation of p38 MAPK.

It has previously been reported that although serine residues and Tyr1045 are essential for EGF-induced receptor ubiquitination, only the serine residues are critical for EGFR internalization and degradation (38). Taking this finding into account, it is probable that the phosphorylation of EGFR at serine residues is critical for the downregulation of EGFR induced by EGCG. The present studies utilizing immunofluorescence microscope (Figure 2) and EGFR tyrosine kinase inhibitors (Figure 3) and the results of our previous study (26) provide evidence that the mechanism of EGCG-induced downregulation of EGFR is different from that of EGF-induced downregulation of the EGFR, whereas with EGF this process involves c-Cbl. The present results also provide strong evidence that phosphorylation of EGFR at serine 1046/1047 via activation of p38 MAPK plays a pivotal role in EGCG-induced downregulation of EGFR. These findings may suggest new therapeutic strategies for inhibiting the proliferation of human cancers that are highly dependent on the function of the EGFR.

It is of interest to summarize our recent studies related the various effects of EGCG on the EGFR in colon cancer cells, with respect to both the time course and the sensitivity to EGCG. The most rapid and sensitive response we have observed is disruption of lipid rafts since this occurred within 5–30 min and with as little as 1–5 μg/ml of EGCG [about one-fourth of the IC_{50} concentration for growth inhibition (25)]. Similar low concentrations of EGCG also induced within 30 min internalization of the EGFR into membrane vesicles (26). Both effects were reversible in washout studies (26). These events were followed by a decrease in phosphorylation of EGFR at ~96 h in cells treated continuously with 1 μg/ml of EGCG or at ~6 h in cells treated with 20 μg/ml of EGCG (6). The present study indicates that 50 μM (~22 μg/ml) of EGCG induces

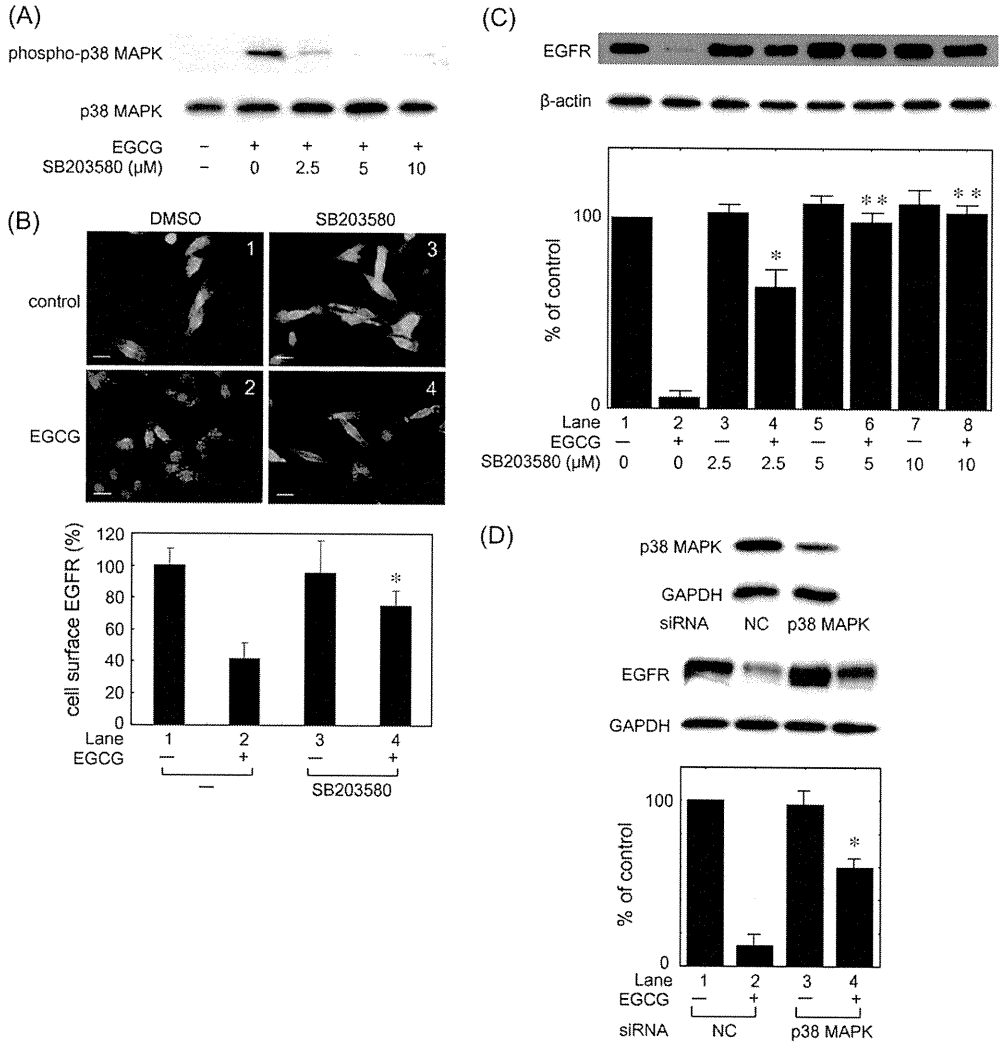

Fig. 5. EGCG-induced downregulation of EGFR was canceled by the inhibition of p38 MAPK. (**A**) SW480 cells were pretreated with the indicated doses of SB203580 for 1 h and then treated with 50 μM of EGCG for 1 h. Protein extracts were then harvested and examined by western blotting using antibodies against phospho-p38 MAPK and p38 MAPK. (**B**) SW480 cells were pretreated with or without 10 μM of SB203580 for 1 h and then labeled for 15 min at 37°C with an anti-EGFR antibody that recognizes the extracellular domain of the EGFR. They were then exposed to EGCG (50 μM) for 30 min at 37°C, followed by fixation with paraformaldehyde. The cells were then treated with an Alexa Fluor 488-conjugated anti-mouse secondary antibody for EGFR (green signal) and 4′,6-diamidino-2-phenylindole (blue signal) and examined by fluorescence microscope. Representative results from at least three independent experiments are shown. Lower bar graph shows the quantification data for cell surface amount of EGFR analyzed by enzyme-linked immunosorbent assay (see details in Materials and Methods). Scale bar indicates 20 μm. (**C**) SW480 cells were pretreated with the indicated doses of SB203580 for 1 h and then exposed the cells to 25 μM of EGCG for 48 h. Protein extracts were then harvested and examined by western blotting using an anti-EGFR antibody. The lower bar graph shows the quantification data for the relative levels of EGFR, after normalization with respect to β-actin, as determined by densitometry. The asterisks indicate significant increase ($^{*}P < 0.05$ and $^{**}P < 0.01$, respectively) as compared with the control (lane 2). (**D**) The cells were incubated with 100 nM of p38 MAPK-siRNA or negative control-siRNA (NC) at 37°C for 48 h in fetal calf serum-free Dulbecco's modified Eagle's medium, followed by exposure to EGCG (25 μM) for 48 h. Protein extracts were then prepared and examined by western blotting using anti-EGFR, p38 MAPK and glyceraldehyde 3-phosphate dehydrogenase (GAPDH). Representative results from triplicate-independent experiments with similar results are shown. The lower bar graph shows the quantification data for the relative levels of EGFR, after normalization with respect to GAPDH, as determined by densitometry. The asterisks indicate significant increase ($^{*}P < 0.05$) as compared with the control (lane 2).

phosphorylation (activation) of p38 MAPK within 10–30 min (Figure 4) and phosphorylation of EGFR at Ser1046/7 within the same time frame (Figure 6C). Degradation of total cellular EGFR occurred even later at ~12 h in cells treated with 25–50 μM of EGCG. Chen *et al.* (39) previously reported that 50 μM of EGCG induces phospho-p38 MAPK in HT29 cells within 1 h, but they did not examine the relationship of this effect to the EGFR. It remains to be determined which of the above inactivating effects of EGCG on the EGFR, or possibly the cascade itself, contributes to the ability of EGCG to inhibit the growth of colon cancer cells. This question is compounded by the multiple additional effects on cancer cells that have been reported for EGCG (39,40).

An important question is the biologic relevance of the present studies since the concentrations of EGCG (50 μM) that activate p38 MAPK are very high compared with the peak plasma concentration of ~0.2 to 0.4 μg/ml (~0.44 to 0.88 μM) in patients administered EGCG (40). However, in clinical studies, patients would receive repeated doses of EGCG over a prolonged period of time,

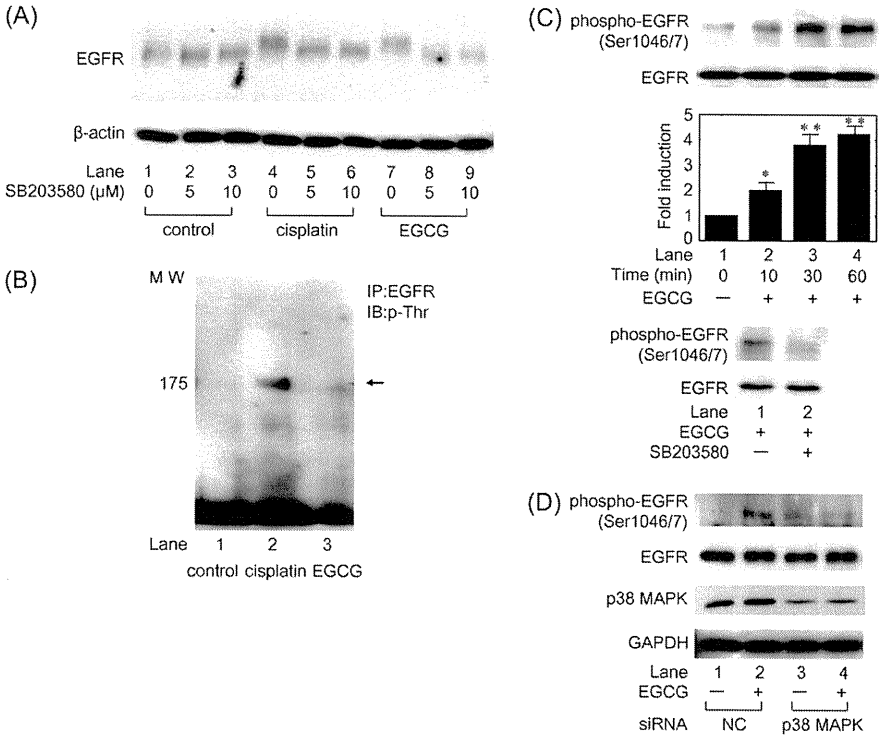

Fig. 6. (**A**) EGCG and cisplatin caused a gel mobility shift of the EGFR and those were canceled by SB203580. The cells were first pretreated with the indicated doses of SB203580 for 1 h and then treated with the control solvent, 100 μM of cisplatin or 25 μM of EGCG for 5 h. The cells were then harvested and the 10 μg of cell lysates were analyzed on a 4% sodium dodecyl sulfate–polyacrylamide gel electrophoresis. An antibody to β-actin was used to control for protein loading. (**B**) EGCG does not phosphorylate EGFR at threonine residues. The cells were first treated with vehicle, 100 μM of cisplatin or 25 μM of EGCG for 5 h. Cell lysates (500 μg each) were prepared and incubated for 12 h at 4°C with an anti-EGFR antibody precoupled to anti-mouse IgG-agarose beads. The bound protein was then analyzed by western blotting with an anti-pan-phospho-threonine (p-Thr) antibody. (**C**) EGCG induces phosphorylation of EGFR at Ser1046/7, which was canceled by SB203580. SW480 cells were treated with 50 μM of EGCG for the indicated times and protein extracts were then harvested and examined by western blotting using an anti-phospho EGFR (Ser1046/7) or an anti-EGFR antibody. The lower bar graph shows the quantification data for the relative levels of phospho-EGFR (Ser1046/7), after normalization with respect to total EGFR, as determined by densitometry. The asterisks indicate significant increase ($^{*}P < 0.05$ and $^{**}P < 0.01$, respectively) as compared with the control (lane 1). In lower panels, SW480 cells were pretreated with or without 10 μM of SB203580 for 1 h and then exposed the cells to 50 μM of EGCG for 30 min. Protein extracts were then harvested and examined by western blotting using an anti-phospho EGFR (Ser1046/7) or an anti-EGFR antibody. (**D**) The cells were incubated with 100 nM of p38 MAPK-siRNA or negative control-siRNA (NC) at 37°C for 48 h in fetal calf serum-free Dulbecco's modified Eagle's medium, followed by exposure to EGCG (50 μM) for 1 h. Protein extracts were then prepared and examined by western blotting using anti-phospho-EGFR (Ser1046/7), anti-EGFR, anti-p38 MAPK and anti-glyceraldehyde 3-phosphate dehydrogenase (GAPDH). Representative results from triplicate-independent experiments with similar results are shown. MW indicates molecular weight.

so there could be an accumulative effect. Indeed, in this and previous cell culture studies, we have found that prolonged exposure of cells to EGCG reduces the concentration required to exert a given effect (6,25,26). Furthermore, there is evidence that EGCG can be concentrated in gastrointestinal tissues (41). Nevertheless, our findings will require confirmation in rodent models or clinical studies with EGCG.

Funding

Grant-in-Aid for Scientific Research from the Ministry of Education, Science, Sports and Culture of Japan (20790490 to A.S.); T.J. Martell Foundation; National Foundation for Cancer Research (to I.B.W.).

Acknowledgements

We are very grateful to Ms Yoko Kawamura for her skillful technical assistance.

Conflict of Interest Statement: None declared.

References

1. Rusch,V. *et al.* (1997) Overexpression of the epidermal growth factor receptor and its ligand transforming growth factor alpha is frequent in resectable non-small cell lung cancer but does not predict tumor progression. *Clin. Cancer Res.*, **3**, 515–522.
2. Masuda,M. *et al.* (2001) Effects of epigallocatechin-3-gallate on growth, epidermal growth factor receptor signaling pathways, gene expression, and chemosensitivity in human head and neck squamous cell carcinoma cell lines. *Clin. Cancer Res.*, **7**, 4220–4229.
3. Fong,C.J. *et al.* (1992) Epidermal growth factor receptor monoclonal antibody inhibits constitutive receptor phosphorylation, reduces autonomous growth, and sensitizes androgen-independent prostatic carcinoma cells to tumor necrosis factor alpha. *Cancer Res.*, **52**, 5887–5892.
4. Pianetti,S. *et al.* (2002) Green tea polyphenol epigallocatechin-3 gallate inhibits Her-2/neu signaling, proliferation, and transformed phenotype of breast cancer cells. *Cancer Res.*, **62**, 652–655.
5. Feng,F.Y. *et al.* (2007) Role of epidermal growth factor receptor degradation in gemcitabine-mediated cytotoxicity. *Oncogene*, **26**, 3431–3439.
6. Shimizu,M. *et al.* (2005) (-)-Epigallocatechin gallate and polyphenon E inhibit growth and activation of the epidermal growth factor receptor